ARTICLE

doi:10.1038/nature15726

Oxidative stress inhibits distant metastasis by human melanoma cells

Elena Piskounova[1], Michalis Agathocleous[1], Malea M. Murphy[1], Zeping Hu[1], Sara E. Huddlestun[1], Zhiyu Zhao[1], A. Marilyn Leitch[2], Timothy M. Johnson[3], Ralph J. DeBerardinis[1] & Sean J. Morrison[1,4]

Solid cancer cells commonly enter the blood and disseminate systemically, but are highly inefficient at forming distant metastases for poorly understood reasons. Here we studied human melanomas that differed in their metastasis histories in patients and in their capacity to metastasize in NOD-SCID-*Il2rg*$^{-/-}$ (NSG) mice. We show that melanomas had high frequencies of cells that formed subcutaneous tumours, but much lower percentages of cells that formed tumours after intravenous or intrasplenic transplantation, particularly among inefficiently metastasizing melanomas. Melanoma cells in the blood and visceral organs experienced oxidative stress not observed in established subcutaneous tumours. Successfully metastasizing melanomas underwent reversible metabolic changes during metastasis that increased their capacity to withstand oxidative stress, including increased dependence on NADPH-generating enzymes in the folate pathway. Antioxidants promoted distant metastasis in NSG mice. Folate pathway inhibition using low-dose methotrexate, ALDH1L2 knockdown, or MTHFD1 knockdown inhibited distant metastasis without significantly affecting the growth of subcutaneous tumours in the same mice. Oxidative stress thus limits distant metastasis by melanoma cells *in vivo*.

Circulating cancer cells are commonly observed in the blood of patients and mice with various cancers[1–4]. However, metastasis is a very inefficient process[5] in which few disseminated cancer cells survive and even fewer proliferate[6–8]. Some patients can have circulating cancer cells in their blood without evidence of metastasis or worse outcomes[9–11].

Epithelial cells undergo cell death when they detach from extracellular matrix in culture as a result of reduced glucose uptake, ATP depletion and oxidative stress[12,13]. Oncogenic signalling can promote their survival by increasing glucose uptake and flux through the pentose phosphate pathway, which generates NADPH and regenerates glutathione, a buffer against oxidative stress[14]. Glutathione is necessary for the initiation of some cancers, and antioxidants can promote cancer initiation and progression[15–18]. Cancer cells thus undergo genetic changes within primary tumours that increase their capacity to withstand oxidative stress, raising the question of whether additional adaptations are required during metastasis. Breast and lung cancer cell lines undergo metabolic changes during invasion in culture and metastasis *in vivo* that would be expected to reduce the generation of reactive oxygen species (ROS)[18–23]. Nonetheless, it is unknown whether ROS levels change in metastasizing cells *in vivo* or whether this limits distant metastasis. In fact, antioxidants inhibit the metastasis of some cancer cell lines, raising the possibility that ROS promotes metastasis in certain contexts[24–26].

We addressed these issues by studying melanomas from several patients that were xenografted into NSG mice. Melanoma metastasis in this assay is predictive of clinical outcome in patients: stage III melanomas that metastasize efficiently in NSG mice go on to form distant metastases in patients, despite surgical resection, whereas melanomas that metastasize inefficiently in mice are usually cured by surgery in patients[27].

Blood and viscera are hostile to metastasis

We obtained four efficiently (UT10, M481, M405 and M514) and four inefficiently (M597, M528, M610 and M498) metastasizing melanomas from patients. All expressed melanoma markers (Extended Data Fig. 1). The efficiently metastasizing melanomas formed distant metastases in patients and in NSG mice after subcutaneous injection (Extended Data Fig. 2a). Conversely, inefficiently metastasizing melanomas did not form distant metastases in patients or macrometastases in NSG mice (Extended Data Fig. 2a).

The efficiently and inefficiently metastasizing melanomas did not significantly differ with regard to the frequency of cells that formed tumours after subcutaneous injection in NSG mice (Table 1) or the rate at which these tumours grew (Extended Data Fig. 2b). One in eight cells from efficiently metastasizing and one in eleven cells from inefficiently metastasizing melanomas formed tumours after subcutaneous injection (Table 1). We often detected circulating melanoma cells by flow cytometry in the blood of mice with efficiently metastasizing, but not inefficiently metastasizing, melanomas (Extended Data Fig. 3a, b).

To test whether the main difference between efficiently and inefficiently metastasizing melanomas is the ability to enter the circulation, we intravenously injected 10, 100, 1,000 or 10,000 cells from efficiently and inefficiently metastasizing melanomas into NSG mice. The melanoma cells were marked by luciferase expression, allowing us to confirm micro- and macrometastases by bioluminescence imaging. Efficiently metastasizing melanomas from all four patients formed macrometastases in several visceral organs (Extended Data Fig. 3c). Limiting dilution analysis indicated that at least 1 in 235 cells formed tumours after intravenous injection (Table 1). By contrast, only 1 in 2,540 cells from inefficiently metastasizing melanomas formed tumours after intravenous injection (Table 1 and Extended Data Fig. 3d). Therefore, the ability to enter circulation is not the only factor that limits distant metastasis.

These data also demonstrate that even efficiently metastasizing melanomas more readily formed tumours after subcutaneous injection (1 in 8 cells) as compared to intravenous injection (1 in 235 cells; Table 1). This was true even when efficiently metastasizing melanoma

[1]Children's Research Institute and the Department of Pediatrics, University of Texas Southwestern Medical Center, Dallas, Texas 75390, USA. [2]Department of Surgery, University of Texas Southwestern Medical Center, Dallas, Texas 75390, USA. [3]Department of Dermatology, University of Michigan, Ann Arbor, Michigan 48109-2216, USA. [4]Howard Hughes Medical Institute, University of Texas Southwestern Medical Center, Dallas, Texas 75390, USA.

Table 1 | Fraction of cells that formed tumours after injection

Melanoma	Subcutaneous	Intravenous	Intrasplenic
Inefficient	1/11	1/2,540 ***	1/3,677 ***
Efficient	1/8	1/235 ***	1/173 ***

The fraction of melanoma cells that formed tumours after subcutaneous, intravenous or intrasplenic injection. Melanoma cells more readily formed tumours after subcutaneous injection (for example, 1 in 8 cells formed tumours) as compared to intravenous (for example, 1 in 235 cells) or intrasplenic (for example, 1 in 173 cells) injection. Limit dilution analysis of data in Extended Data Fig. 3 to infer the minimum frequency of tumour-forming melanoma cells after subcutaneous, intravenous or intrasplenic transplantation into NSG mice. Each mean value reflects 5 (subcutaneous), 10 (intravenous), or 4 (intrasplenic) independent experiments using melanomas obtained from 8 different patients (see details in Extended Data Fig. 3). Statistical significance was assessed by a Chi-square test using the ELDA software[46] (***$P < 0.0001$).

cells were injected subcutaneously without Matrigel (1 in 60 cells formed tumours; $P < 0.001$). This suggests that the blood was more hostile to melanoma cells than the subcutaneous environment.

If distant metastasis is limited mainly by survival in the blood, direct injection into a visceral organ should increase tumour formation. To test this, we injected efficiently and inefficiently metastasizing melanomas into the spleens of NSG mice. Efficiently metastasizing melanomas from two out of three patients formed macrometastases in several visceral organs in most mice (Extended Data Fig. 3e and Table 1; at least 1 in 173 cells formed tumours after intrasplenic injection). By contrast, only 1 in 3,677 cells from inefficiently metastasizing melanomas formed tumours after intrasplenic injection (Extended Data Fig. 3f and Table 1). The ability to survive in the circulation is therefore not the only factor that limits distant metastasis. The spleen is also a relatively hostile environment for melanoma cells.

Reversible tropic changes during metastasis

To test whether melanoma cells undergo changes in properties during metastasis, we obtained efficiently metastasizing melanoma cells from 12 donor mice that had been grafted with melanomas from 3 patients (M481, M405 and UT10). We compared the capacity of melanoma cells from subcutaneous tumours versus the blood versus metastatic liver nodules (2–5 mm in diameter) in the same donor mice to form tumours after subcutaneous, intravenous or intrasplenic injection in recipient mice (Table 2a; see Extended Data Fig. 3g for experimental design). After subcutaneous injection, melanoma cells from subcutaneous tumours were significantly better at forming tumours (1 in 14 cells formed tumours) than melanoma cells from the blood (1 in 63 cells) or metastatic nodules (1 in 55 cells; Table 2a). By contrast, after intrasplenic injection, melanoma cells from metastatic nodules were significantly better at forming tumours (1 in 130 cells) than melanoma cells from the blood (1 in 372 cells) or subcutaneous tumours (1 in 708 cells; Table 2a). This suggests melanoma cells adapt to the sites of metastasis as they metastasize.

To test whether the changes were irreversible (for example, genetic) or reversible (for example, epigenetic or metabolic), we tested whether small numbers of metastatic melanoma cells would reacquire subcutaneous properties after being passaged subcutaneously for a short period of time. We subcutaneously transplanted 100 cells from subcutaneous tumours, the blood or metastatic liver nodules of the same donor mice into primary recipient mice and allowed them to form tumours for up to 12 weeks (Table 2b; all injections formed tumours). Then we retransplanted melanoma cells from the subcutaneous tumours into subcutaneous, intravenous or intrasplenic sites in secondary recipient mice (Extended Data Fig. 3h shows experimental design). Melanoma cells that originated in all sites formed subcutaneous tumours with high efficiency in secondary recipient mice after being passaged subcutaneously (Table 2b). Melanoma cells that originated in all sites formed metastatic tumours with low efficiency after intravenous or intrasplenic injections in secondary recipient mice after being passaged subcutaneously (Table 2b). The changes in tumorigenic tropism during metastasis are thus reversible. Since these reversible changes were observed very consistently, even in small numbers of melanoma cells, these changes cannot reflect selection for rare genetic events during metastasis followed by reversion mutations after subcutaneous re-transplantation.

Oxidative stress limits distant metastasis

We performed liquid chromatography–tandem mass spectrometry (LC–MS/MS) metabolomics on subcutaneous tumours and visceral metastatic nodules from the same NSG mice transplanted with efficiently metastasizing melanomas derived from four patients. In two independent experiments, unsupervised clustering of metabolomics

Table 2 | Melanoma cells undergo reversible changes in tropism during metastasis

a Transplantation in primary recipient mice

Source of melanoma cells in donor mice	Transplantation site in primary recipient mice	Tumorigenic frequency
Subcutaneous tumour cells	Subcutaneous	1/14 ***
Circulating cells		1/63 ***
Metastatic nodules		1/55 ***
Subcutaneous tumour cells	Intravenous	1/1,282
Circulating cells		1/4,270
Metastatic nodules		1/627
Subcutaneous tumour cells	Intrasplenic	1/708
Circulating cells		1/372 **
Metastatic nodules		1/130 *

b Transplantation in secondary recipient mice

Source of melanoma cells in donor mice	Passage site in primary recipient mice	Transplantation site in secondary recipient mice	Tumorigenic frequency
Subcutaneous tumour cells	Subcutaneous	Subcutaneous	1/11
Circulating cells			1/17
Metastatic nodules			1/11
Subcutaneous tumour cells	Subcutaneous	Intravenous	1/584
Circulating cells			1/566
Metastatic nodules			1/899
Subcutaneous tumour cells	Subcutaneous	Intrasplenic	1/843
Circulating cells			1/307
Metastatic nodules			1/584

a, Limiting dilution analysis of the fraction of melanoma cells from subcutaneous tumours, the blood (circulating cells), or metastatic nodules that formed tumours after subcutaneous, intravenous, or intrasplenic transplantation. These data reflect three independent experiments performed with efficiently metastasizing melanomas (M405, M481 and UT10; $n = 10$ mice/melanoma/melanoma cell source/transplantation site for a total of 270 mice).

b, Limiting dilution analysis of the fraction of melanoma cells from subcutaneous tumours, the blood (circulating cells), or metastatic nodules that formed tumours after being passaged subcutaneously in primary recipient mice and then transplanted subcutaneously, intravenously, or intrasplenically into secondary recipient mice. These data reflect one experiment performed with efficiently metastasizing melanoma cells (M481; $n = 8$–10 mice/melanoma cell source/transplantation site for a total of 85 mice).

Statistical significance was assessed by a Chi-square test using ELDA software[46]. *$P < 0.05$; **$P < 0.005$; ***$P < 0.0005$.

data showed that metastatic nodules obtained from the liver, pancreas and kidney almost always clustered together, distinct from subcutaneous tumours, irrespective of the xenograft line (Extended Data Fig. 4a, b; complete metabolomics data are shown in Extended Data Tables 1 and 2). Among subcutaneous tumours and among metastatic nodules, samples clustered by patient. We obtained similar results when melanoma cells were isolated by flow cytometry, excluding mouse cells (Extended Data Fig. 4c). The metabolic differences between subcutaneous tumours and visceral metastases appeared to be largely reversible as metabolomics analysis of tumours from Table 2b showed that subcutaneous tumours clustered together irrespective of whether they arose from the transplantation of subcutaneous, circulating or metastatic cells (Extended Data Fig. 4d, e).

In a total of six independent experiments that involved four different technical approaches, the glutathione (GSH) to oxidized glutathione (GSSG) ratio was always significantly higher in subcutaneous tumours than in metastatic nodules or circulating melanoma cells (Fig. 1a, b and Extended Data Fig. 4f). This was true irrespective of whether melanoma cells were isolated by dissection or by flow cytometry (to eliminate stromal cells). The lower GSH/GSSG ratio in circulating melanoma cells and metastatic nodules suggested that metastasizing cells experienced oxidative stress not observed in established subcutaneous tumours, and they consumed GSH in an effort to maintain redox homeostasis.

Consistent with this, cytoplasmic ROS levels were significantly higher in circulating melanoma cells and visceral metastatic nodules than in subcutaneous tumours (Fig. 1c). Mitochondrial ROS levels were significantly higher in visceral metastatic nodules than in circulating melanoma cells and subcutaneous tumours (Fig. 1d).

Mitochondrial respiration is one of the main sources of ROS. Mitochondrial mass declined significantly in circulating melanoma cells and metastatic nodules as compared to subcutaneous tumours (Fig. 1e). Mitochondrial membrane potential also declined significantly in circulating melanoma cells as compared to subcutaneous tumours but not in metastatic nodules (Fig. 1f). These data raised the possibility that mitochondrial function is reduced in circulating melanoma cells in an effort to reduce ROS generation.

These changes in redox status between subcutaneous and metastasizing cells appeared to be reversible. Even though the GSH/GSSG ratio was always higher in subcutaneous tumours than in metastatic nodules, the GSH/GSSG ratio in subcutaneous tumours derived from the transplantation of metastatic cells was even higher than the GSH/GSSG ratio in subcutaneous tumours derived from the transplantation of subcutaneous cells (Extended Data Fig. 4g).

Changes in mitochondrial mass between subcutaneous and metastatic melanoma cells were also reversible. Subcutaneous tumours always exhibited significantly higher mitochondrial mass than metastatic nodules, irrespective of whether the subcutaneous tumours arose from the transplantation of subcutaneous tumour cells, circulating cells or metastatic cells (Fig. 1g and Extended Data Fig. 4h).

To test whether oxidative stress limits melanoma metastasis, we subcutaneously transplanted efficiently metastasizing melanoma cells derived from three patients into NSG mice and treated the mice with daily subcutaneous injections of the antioxidant *N*-acetyl-cysteine (NAC; 200 mg kg^{-1} day^{-1}). In no case did NAC treatment significantly affect the growth of established subcutaneous tumours (Fig. 2a), but it significantly increased the frequency of melanoma cells in the blood of mice transplanted with M405 and UT10 (Fig. 2b), and significantly increased metastatic disease burden in mice with all three melanomas (Fig. 2c). Oxidative stress therefore limits the metastasis of melanoma cells *in vivo*.

Among efficiently metastasizing melanomas from three patients, NAC pre-treatment of cells and administration to mice increased tumour formation after intravenous injection by tenfold ($P < 0.0001$; Extended Data Table 3a). Among inefficiently metastasizing melanomas from two patients, tumours only arose from cells treated with NAC (Extended Data Table 3b). Oxidative stress thus limits tumorigenesis by circulating melanoma cells.

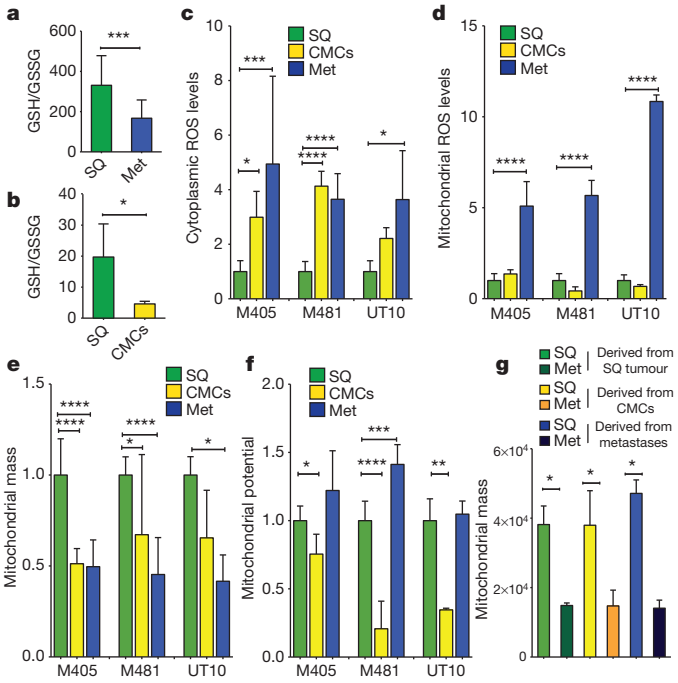

Figure 1 | Metastasizing melanoma cells experience high levels of oxidative stress. **a**, GSH/GSSG ratio in subcutaneous tumours (SQ) as compared to metastatic nodules (Met) ($n = 15$ mice from two independent experiment with three melanomas (M481, M405 and UT10); note that extractions were performed with 0.1% formic acid to prevent spontaneous oxidation[47]). Total amounts of GSH and GSSG are shown in Extended Data Fig. 5h, i. **b**, GSH/GSSG ratio in subcutaneous tumours as compared to circulating melanoma cells ($n = 7$ mice from three independent experiments with two melanomas (M405 and UT10); these were different experiments than those in **a**, performed under different technical conditions). **c**, **d**, Cytoplasmic (**c**) and mitochondrial (**d**) ROS levels in dissociated melanoma cells from subcutaneous tumours, the blood (circulating melanoma cells, CMCs), and metastatic nodules obtained from the same mice ($n = 9$ mice from three independent experiments using three different melanomas). **e**, **f**, Mitochondrial mass (**e**) and mitochondrial membrane potential (**f**) in dissociated melanoma cells from subcutaneous tumours, the blood, and metastatic nodules obtained from the same mice ($n = 6$ mice from two independent experiments using three different melanomas). **g**, Melanoma cells underwent reversible changes in mitochondrial mass during metastasis: mitochondrial mass in dissociated melanoma cells from subcutaneous tumours versus metastatic nodules obtained from the same mice transplanted with subcutaneous, circulating or metastatic melanoma cells. All data represent mean ± s.d. Statistical significance was assessed using two-tailed Student's *t*-tests (**a** and **b**) and one-way analyses of variance (ANOVAs) followed by Dunnett's tests for multiple comparisons (**c**–**g**). $*P < 0.05$; $***P < 0.0005$; $****P < 0.00005$.

Metabolic adaptations during metastasis

We proposed that successfully metastasizing cells undergo reversible metabolic changes that increase their capacity to withstand oxidative stress. One such adaptation that could promote survival would be increased GSH regeneration[28–30]. NADPH is needed to convert GSSG into GSH and increased production of NADPH promotes the regeneration of GSH[28–30]. In fact, we observed significantly higher levels of NADPH and NADP in metastatic cells than in subcutaneous tumours (Fig. 2d, e). The NADPH/NADP ratio was significantly reduced in metastases as compared to subcutaneous tumours for one melanoma (M481) but not for a second (UT10; Extended Data Fig. 5e). The higher levels of NADPH in metastases raised the possibility that metastasizing cells generate more NADPH to increase their capacity to regenerate GSH. The oxidative stress in these cells would be predicted to consume more NADPH, potentially explaining

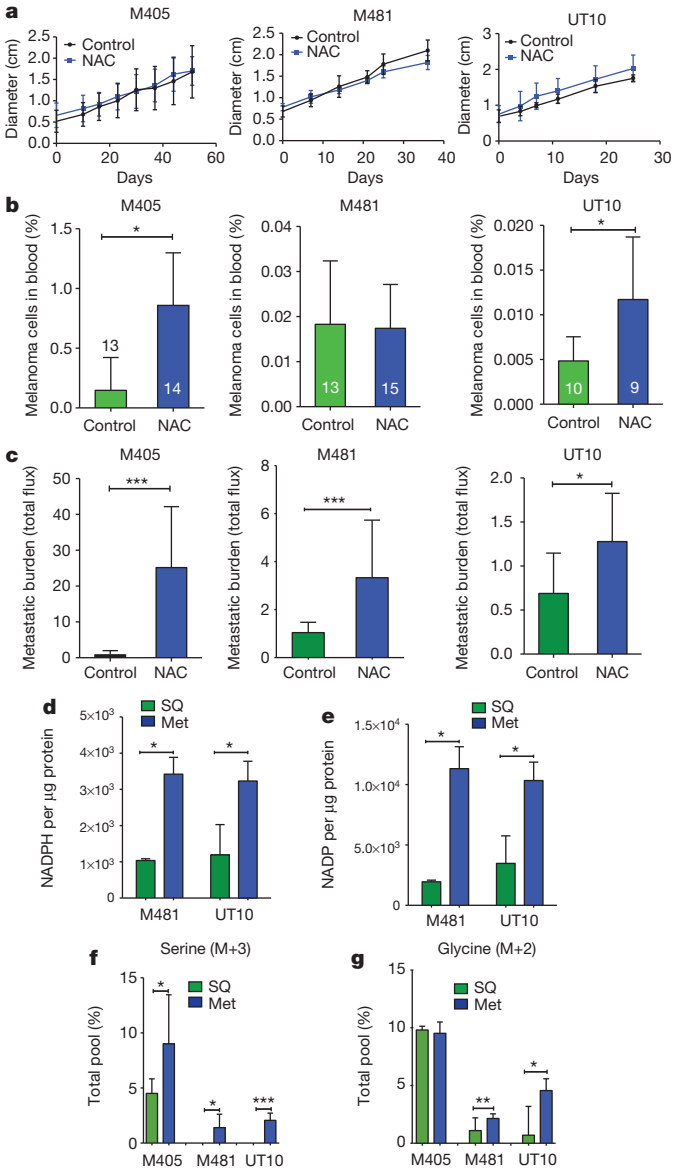

Figure 2 | Melanoma cell metastasis, but not subcutaneous tumour growth, is promoted by antioxidants *in vivo*. **a**–**c**, Growth of established subcutaneous tumours in NSG mice treated with either PBS (control) or NAC by daily subcutaneous injection. Tumour diameter source data are shown in Supplementary Fig. 1. Frequency of circulating melanoma cells in the blood (**b**) and metastatic disease burden (**c**) assessed based on total bioluminescence signal from the visceral organs of the same mice. Data in **a**–**c** represent eight independent experiments, with total replicates/treatment shown in the bars of **b**. A single representative experiment per melanoma is shown in **a** owing to the difficulty of reflecting tumour growth measurements from independent experiments in the same graph. No statistically significant differences among treatments were observed in subcutaneous tumour growth in any experiment. **d**, **e**, Levels of NADPH (**d**) and NADP (**e**) in subcutaneous tumours versus metastatic nodules ($n = 4$ mice from two independent experiments with M481 and UT10). **f**, **g**, *In vivo* isotope tracing of uniformly ^{13}C-labelled glucose into serine (**f**) and glycine (**g**) in subcutaneous tumours versus metastatic nodules from the same mice ($n = 6$ mice in two independent experiments for M405; $n = 3$ mice in one experiment for each of M481 and UT10). The fragments for uniformly labelled serine (M + 3) and glycine (M + 2), which come from labelled glucose via *de novo* serine synthesis, are shown. All data represent mean ± s.d. Statistical significance was assessed using two-tailed Student's *t*-tests (**d**–**f**, **h** and **i**), or the Mann–Whitney test (**g**, due to unequal variance), and repeated-measures two-way ANOVAs (**a**–**c**). *$P < 0.05$; **$P < 0.005$; ***$P < 0.0005$; ****$P < 0.00005$.

why the NADPH/NADP ratio did not necessarily change despite increases in the amounts of NADPH and NADP.

Metastatic nodules had high levels of purine intermediates relative to subcutaneous tumours in the same mice (Extended Data Tables 1 and 2). This could reflect changed folate pathway activity. Moreover, folate metabolism is a major source of NADPH for oxidative stress management[29–31], raising the question of whether the folate pathway promotes distant metastasis. NADPH regeneration by the folate pathway involves the conversion of serine to glycine and the donation of a methyl group to tetrahydrofolate (see Extended Data Fig. 5j). Serine can be imported into cells as well as produced *de novo* from glucose via the glycolytic intermediate 3-phosphoglycerate (3-PG). Increased *de novo* serine synthesis promotes the growth of some melanomas and breast cancers[32,33]. To test for alterations of these pathways during metastasis, we administered uniformly ^{13}C-labelled glucose to NSG mice bearing melanomas derived from three patients. We observed significantly increased ^{13}C-labelling of serine and glycine in metastatic tumours as compared to subcutaneous tumours (Fig. 3f, g and Extended Data Fig. 5c, d). However, we observed no differences between subcutaneous tumours and metastases in terms of the fractional enrichments of uniformly labelled lactate or 3-PG, the precursor used for *de novo* serine synthesis (Extended Data Fig. 5a, b). Metastatic tumours thus display enhanced contribution of glucose carbon to tissue serine and glycine levels, suggesting increased flux through the folate pathway.

Western blotting and immunofluorescence analysis of key enzymes in the folate pathway showed a striking increase in the expression of the NADPH-regenerating enzyme ALDH1L2 in liver, pancreas and lung metastases compared to subcutaneous tumours, although not in kidney metastases (Fig. 3a and Extended Data Fig. 6). Some metastases also showed reduced expression of an NADPH-consuming folate metabolism enzyme, MTHFR (Fig. 3a). The expression of other folate metabolism enzymes did not consistently change during metastasis, nor did a variety of other enzymes in antioxidant pathways (Fig. 3a and Extended Data Table 4).

We compared ALDH1L2 levels in subcutaneous tumours versus metastatic nodules from mice transplanted with subcutaneous, circulating or metastatic melanoma cells. ALDH1L2 was much more highly expressed in liver nodules than in subcutaneous tumours in both donor and recipient mice, irrespective of whether the subcutaneous tumours arose from subcutaneous, circulating or metastatic melanoma cells (Fig. 3h). The changes in ALDH1L2 expression during metastasis were thus reversible.

To test whether metastasizing cells are more dependent than subcutaneous cells on the folate pathway, we transplanted melanoma cells from three patients subcutaneously in NSG mice and treated with a low dose of methotrexate (1.25 mg kg^{-1} day^{-1}), an inhibitor of dihydrofolate reductase (Extended Data Fig. 5j). We simultaneously provided thymidine (3 mg kg^{-1} day^{-1}) and hypoxanthine (750 µg mg^{-1} day^{-1}) to the mice to ameliorate the effects of folate pathway inhibition on nucleotide metabolism. Methotrexate treatment in these conditions had no significant effect on the growth of subcutaneous tumours (Fig. 3b); however, the frequency of circulating melanoma cells in the blood of the same mice was significantly reduced (Fig. 3c), as was metastatic disease burden (Fig. 3d), in mice bearing all three melanomas. Metastasizing melanoma cells are therefore particularly sensitive to folate pathway inhibition.

Depletion of ALDH1L2 can decrease the GSH/GSSG ratio *in vitro*[30]. To test whether ALDH1L2 is required for metastasis, we identified two short hairpin RNAs (shRNAs) that knocked down ALDH1L2 expression in melanoma cells (Extended Data Fig. 5f). We infected melanoma cells derived from three patients with either of these shRNAs or a scrambled control shRNA, then injected the cells subcutaneously in NSG mice. Neither of the shRNAs against ALDH1L2 significantly affected the growth of subcutaneous tumours (Fig. 3e), but both shRNAs significantly reduced the frequency of circulating melanoma

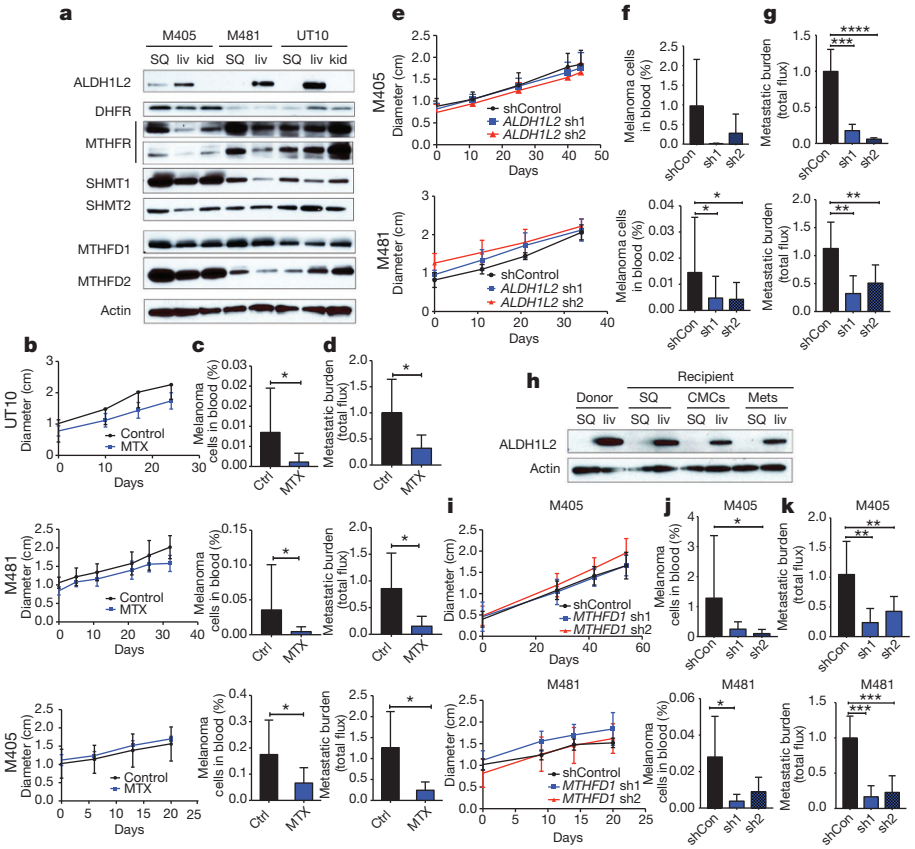

Figure 3 | During metastasis, some melanoma cells reversibly increase their expression of folate pathway enzymes that generate NADPH and folate pathway inhibition selectively impairs metastasis. **a**, Western blot analysis of folate pathway enzymes in subcutaneous tumours versus metastatic liver (liv) and kidney (kid) nodules from NSG mice transplanted with three different melanomas. **b**–**d**, Growth of subcutaneous tumours in mice bearing three different melanomas (M405, M481 and UT10) treated with dimethylsulfoxide (DMSO; control (ctrl)) or methotrexate (MTX) ($n = 5$ mice per treatment). The frequency of circulating melanoma cells in the blood (**c**) and metastatic disease burden (**d**) in the same mice ($n = 10$ mice per treatment for each melanoma except $n = 8$ for M405). Data in **b**–**d** reflect six independent experiments, but only one representative experiment per melanoma is shown in **b**. **e**–**g**, Growth of subcutaneous tumours in mice transplanted with two different melanomas expressing scrambled control shRNA versus two shRNAs against *ALDH1L2*. The frequency of circulating melanoma cells (**f**) and metastatic disease burden in visceral organs based on total bioluminescence signal (**g**). The data in **e**–**g** reflect six independent experiments ($n = 10$ mice per shRNA for M405 and $n = 19$ mice per shRNA for M481), but only one representative experiment per melanoma is shown in **e**. **h**, Western blot analysis of ALDH1L2 expression in subcutaneous tumours versus metastatic liver nodules from a donor mouse or from recipient mice subcutaneously transplanted with subcutaneous, circulating or metastatic melanoma cells from the donor mouse. The increase in ALDH1L2 expression in metastatic liver nodules was reversible after subcutaneous transplantation. Data in **a** and **h** are from two independent experiments. **i**–**k**, Growth of subcutaneous tumours in mice transplanted with cells from two melanomas expressing either scrambled control shRNAs or two shRNAs against *MTHFD1*. Frequency of circulating melanoma cells (**j**) and metastatic disease burden in visceral organs (**k**) from the same mice. Data in **i**–**k** reflect four independent experiments, with a total of nine mice per control shRNA and ten mice per shRNA against *MTHFD1* for each melanoma. One representative experiment per melanoma is shown in **i**. All error bars represent s.d. Statistical significance was assessed using ANOVA followed by Dunnett's test for multiple comparisons (**f**, **g**, **j** and **k**), two-tailed Student's *t*-tests (**c** and **d**) and repeated measures two-way ANOVAs (**b**, **e** and **i**). $*P < 0.05$; $**P < 0.005$, $***P < 0.0005$; $****P < 0.00005$. Tumour diameter and western blot source data are in Supplementary Fig. 1.

cells in the blood of mice bearing one of two melanomas (Fig. 3f) and overall metastatic disease burden in both melanomas (Fig. 3g). ALDH1L2 thus promotes melanoma metastasis *in vivo*.

We performed a similar experiment on another NADPH-regenerating enzyme in the folate pathway, MTHFD1 (Extended Data Fig. 5j). We identified two shRNAs that knocked down MTHFD1 expression in melanoma cells (Extended Data Fig. 5g). Neither shRNA against MTHFD1 significantly affected the growth of subcutaneous tumours (Fig. 3i), but they both reduced the frequencies of circulating melanoma cells in the blood (Fig. 3j) and metastatic disease burden in mice bearing both melanomas (Fig. 3k). MTHFD1 thus promotes melanoma metastasis *in vivo*.

Our results suggest that few circulating cancer cells survive and proliferate[6–8] because of oxidative stress. Our results further suggest that metabolic pathways that regenerate NAPDH and buffer oxidative stress represent therapeutic targets to impede distant metastasis. Metastasizing melanoma cells are more dependent on certain NADPH-regenerating folate pathway enzymes than subcutaneous melanoma cells. However, these enzymes cannot account for the increase in NADP in metastatic nodules as compared to subcutaneous tumours (Fig. 2d, e). Therefore, metastasizing cells probably also undergo additional metabolic changes that promote the generation of NADP and NADPH.

Changes in the expression of individual folate pathway enzymes are unlikely to be sufficient to drive metastasis. Since the key changes driving distant metastasis were reversible adaptations rather than stochastic genetic changes, there is no reason why these changes would need to be driven by a single sufficient driver. Adaptive changes might involve coordinated changes in the expression of several enzymes to increase flux through metabolic pathways. Other metabolic pathways also contribute to the synthesis and regeneration of NADPH, including the pentose phosphate[12,13] and malate[34] pathways. These pathways could potentially also contribute to the ability of melanoma cells to survive during metastasis.

Our experiments showed that oxidative stress increases in metastasizing cells as compared to established subcutaneous tumours and

limits distant metastasis. However, we did not test whether oxidative stress also limits the initiation and early growth of primary cutaneous melanomas. Thus, transient oxidative stress could occur during the formation of primary tumours[15–18] in addition to limiting distant metastasis at a later stage of cancer progression.

ROS can cause oncogenic mutations and activate oncogenic pathways, raising the possibility that treatment with antioxidants could suppress the initiation or progression of some cancers[28,35]. Antioxidants or antioxidant enzymes suppress cancer initiation in some contexts[36–38] while increasing cancer initiation in other contexts[15–17,39]. Increasing dietary antioxidants has generally not reduced cancer incidence in clinical trials[40]. Dietary supplementation with antioxidants actually increased incidence and death from lung and prostate cancer[41–43]. Dietary supplementation with folate promotes the development and progression of breast cancer[44,45]. Our results suggest that antioxidants promote disease progression, at least in melanoma, by promoting metastasis.

Online Content Methods, along with any additional Extended Data display items and Source Data, are available in the online version of the paper; references unique to these sections appear only in the online paper.

Received 25 December 2014; accepted 17 September 2015.
Published online 14 October 2015.

1. Yu, M. *et al.* Circulating breast tumor cells exhibit dynamic changes in epithelial and mesenchymal composition. *Science* **339,** 580–584 (2013).
2. Stott, S. L. *et al.* Isolation and characterization of circulating tumor cells from patients with localized and metastatic prostate cancer. *Sci. Transl. Med.* **2,** 25ra23 (2010).
3. Yu, M. *et al.* Cancer therapy. *Ex vivo* culture of circulating breast tumor cells for individualized testing of drug susceptibility. *Science* **345,** 216–220 (2014).
4. Nagrath, S. *et al.* Isolation of rare circulating tumour cells in cancer patients by microchip technology. *Nature* **450,** 1235–1239 (2007).
5. Vanharanta, S. & Massague, J. Origins of metastatic traits. *Cancer Cell* **24,** 410–421 (2013).
6. Luzzi, K. J. *et al.* Multistep nature of metastatic inefficiency: dormancy of solitary cells after successful extravasation and limited survival of early micrometastases. *Am. J. Pathol.* **153,** 865–873 (1998).
7. Cameron, M. D. *et al.* Temporal progression of metastasis in lung: cell survival, dormancy, and location dependence of metastatic inefficiency. *Cancer Res.* **60,** 2541–2546 (2000).
8. Kienast, Y. *et al.* Real-time imaging reveals the single steps of brain metastasis formation. *Nature Med.* **16,** 116–122 (2010).
9. Engell, H. C. Cancer cells in the blood; a five to nine year follow up study. *Ann. Surg.* **149,** 457–461 (1959).
10. Griffiths, J. D., McKinna, J. A., Rowbotham, H. D., Tsolakidis, P. & Salsbury, A. J. Carcinoma of the colon and rectum: circulating malignant cells and five-year survival. *Cancer* **31,** 226–236 (1973).
11. Salsbury, A. J. The significance of the circulating cancer cell. *Cancer Treat. Rev.* **2,** 55–72 (1975).
12. Debnath, J. & Brugge, J. S. Modelling glandular epithelial cancers in three-dimensional cultures. *Nature Rev. Cancer* **5,** 675–688 (2005).
13. Debnath, J. *et al.* The role of apoptosis in creating and maintaining luminal space within normal and oncogene-expressing mammary acini. *Cell* **111,** 29–40 (2002).
14. Schafer, Z. T. *et al.* Antioxidant and oncogene rescue of metabolic defects caused by loss of matrix attachment. *Nature* **461,** 109–113 (2009).
15. Harris, I. S. *et al.* Glutathione and thioredoxin antioxidant pathways synergize to drive cancer initiation and progression. *Cancer Cell* **27,** 211–222 (2015).
16. Sayin, V. I. *et al.* Antioxidants accelerate lung cancer progression in mice. *Sci. Transl. Med.* **6,** 221ra215 (2014).
17. DeNicola, G. M. *et al.* Oncogene-induced Nrf2 transcription promotes ROS detoxification and tumorigenesis. *Nature* **475,** 106–109 (2011).
18. Dey, S. *et al.* ATF4-dependent induction of heme oxygenase 1 prevents anoikis and promotes metastasis. *J. Clin. Invest.* **125,** 2592–2608 (2015).
19. Dong, C. *et al.* Loss of FBP1 by Snail-mediated repression provides metabolic advantages in basal-like breast cancer. *Cancer Cell* **23,** 316–331 (2013).
20. Kamarajugadda, S. *et al.* Manganese superoxide dismutase promotes anoikis resistance and tumor metastasis. *Cell Death Dis.* **4,** e504 (2013).
21. Qu, Y. *et al.* Thioredoxin-like 2 regulates human cancer cell growth and metastasis via redox homeostasis and NF-κB signaling. *J. Clin. Invest.* **121,** 212–225 (2011).
22. Chen, E. I. *et al.* Adaptation of energy metabolism in breast cancer brain metastases. *Cancer Res.* **67,** 1472–1486 (2007).
23. Lu, X., Bennet, B., Mu, E., Rabinowitz, J. & Kang, Y. Metabolomic changes accompanying transformation and acquisition of metastatic potential in a syngeneic mouse mammary tumor model. *J. Biol. Chem.* **285,** 9317–9321 (2010).
24. Porporato, P. E. *et al.* A mitochondrial switch promotes tumor metastasis. *Cell Rep.* **8,** 754–766 (2014).
25. LeBleu, V. S. *et al.* PGC-1α mediates mitochondrial biogenesis and oxidative phosphorylation in cancer cells to promote metastasis. *Nature Cell Biol.* **16,** 992–1003 (2014).
26. Ishikawa, K. *et al.* ROS-generating mitochondrial DNA mutations can regulate tumor cell metastasis. *Science* **320,** 661–664 (2008).
27. Quintana, E. *et al.* Human melanoma metastasis in NSG mice correlates with clinical outcome in patients. *Sci. Transl. Med.* **4,** 159ra149 (2012).
28. Gorrini, C., Harris, I. S. & Mak, T. W. Modulation of oxidative stress as an anticancer strategy. *Nature Rev. Drug Discov.* **12,** 931–947 (2013).
29. Lewis, C. A. *et al.* Tracing compartmentalized NADPH metabolism in the cytosol and mitochondria of mammalian cells. *Mol. Cell* **55,** 253–263 (2014).
30. Fan, J. *et al.* Quantitative flux analysis reveals folate-dependent NADPH production. *Nature* **510,** 298–302 (2014).
31. Ye, J. *et al.* Serine catabolism regulates mitochondrial redox control during hypoxia. *Cancer Discovery* **4,** 1406–1417 (2014).
32. Locasale, J. W. *et al.* Phosphoglycerate dehydrogenase diverts glycolytic flux and contributes to oncogenesis. *Nature Genet.* **43,** 869–874 (2011).
33. Possemato, R. *et al.* Functional genomics reveal that the serine synthesis pathway is essential in breast cancer. *Nature* **476,** 346–350 (2011).
34. Jiang, P., Du, W., Mancuso, A., Wellen, K. E. & Yang, X. Reciprocal regulation of p53 and malic enzymes modulates metabolism and senescence. *Nature* **493,** 689–693 (2013).
35. Chandel, N. S. & Tuveson, D. A. The promise and perils of antioxidants for cancer patients. *N. Engl. J. Med.* **371,** 177–178 (2014).
36. Gao, P. *et al.* HIF-dependent antitumorigenic effect of antioxidants *in vivo*. *Cancer Cell* **12,** 230–238 (2007).
37. Teoh-Fitzgerald, M. L., Fitzgerald, M. P., Zhong, W., Askeland, R. W. & Domann, F. E. Epigenetic reprogramming governs EcSOD expression during human mammary epithelial cell differentiation, tumorigenesis and metastasis. *Oncogene* **33,** 358–368 (2014).
38. Glasauer, A. & Chandel, N. S. Targeting antioxidants for cancer therapy. *Biochem. Pharmacol.* **92,** 90–101 (2014).
39. Glasauer, A., Sena, L. A., Diebold, L. P., Mazar, A. P. & Chandel, N. S. Targeting SOD1 reduces experimental non-small-cell lung cancer. *J. Clin. Invest.* **124,** 117–128 (2014).
40. Fortmann, S. P. *et al.* Vitamin, mineral, and multivitamin supplements for the primary prevention of cardiovascular disease and cancer: a systematic evidence review for the U.S. preventive services task force U.S. preventive services task force. *Ann Intern Med.* **159,** 824–834 (2013).
41. The Alpha-Tocopherol, Beta Carotene Cancer Prevention Study Group. The effect of vitamin E and beta carotene on the incidence of lung cancer and other cancers in male smokers. *N. Engl. J. Med.* **330,** 1029–1035 (1994).
42. Klein, E. A. *et al.* Vitamin E and the risk of prostate cancer: the Selenium and Vitamin E Cancer Prevention Trial (SELECT). *J. Am. Med. Assoc.* **306,** 1549–1556 (2011).
43. Goodman, G. E. *et al.* The Beta-Carotene and Retinol Efficacy Trial: incidence of lung cancer and cardiovascular disease mortality during 6-year follow-up after stopping beta-carotene and retinol supplements. *J. Natl. Cancer Inst.* **96,** 1743–1750 (2004).
44. Deghan Manshadi, S. *et al.* Folic acid supplementation promotes mammary tumor progression in a rat model. *PLoS ONE* **9,** e84635 (2014).
45. Ebbing, M. *et al.* Cancer incidence and mortality after treatment with folic acid and vitamin B12. *J. Am. Med. Assoc.* **302,** 2119–2126 (2009).
46. Hu, Y. & Smyth, G. K. ELDA: extreme limiting dilution analysis for comparing depleted and enriched populations in stem cell and other assays. *J. Immunol. Methods* **347,** 70–78 (2009).

Supplementary Information is available in the online version of the paper.

Acknowledgements S.J.M. is a Howard Hughes Medical Institute (HHMI) Investigator, the Mary McDermott Cook Chair in Pediatric Genetics, the director of the Hamon Laboratory for Stem Cells and Cancer, and a Cancer Prevention and Research Institute of Texas Scholar. We thank K. Correll and M. Gross for mouse colony management; N. Loof and the Moody Foundation Flow Cytometry Facility. We thank N. Meireles and the University of Michigan Melanoma Biobank, for Biobank database and melanoma clinical data management.

Author Contributions E.P. and S.J.M. conceived the project, designed, and interpreted experiments. M.A. and R.J.D. participated in the design and interpretation of experiments related to metabolic mechanisms. E.P. performed all the experiments with technical assistance from S.E.H., metabolomics assistance from M.A and imaging assistance from M.M.M. Z.H. and M.A developed metabolomics methods. Z.Z. assisted with statistical analyses. A.M.L. and T.M.J. provided melanoma specimens and associated clinical data. E.P., M.A. and S.J.M wrote the manuscript.

Author Information Reprints and permissions information is available at www.nature.com/reprints. The authors declare no competing financial interests. Readers are welcome to comment on the online version of the paper. Correspondence and requests for materials should be addressed to S.J.M. (sean.morrison@utsouthwestern.edu).

METHODS

Obtaining melanomas and enzymatic dissociation. Melanoma specimens were obtained with informed consent from all patients according to protocols approved by the Institutional Review Boards of the University of Michigan Medical School (IRBMED approvals HUM00050754 and HUM00050085; see ref. 27) and the University of Texas Southwestern Medical Center. Tumours were dissociated in Sterile Closed System Tissue Grinders (SKS Science) in enzymatic digestion medium containing 200 U ml^{-1} collagenase IV (Worthington) for 20 min at 37 °C. DNase (50–100 U ml^{-1}) was added to reduce clumping of cells during digestion. Cells were filtered with a 40- μm cell strainer to obtain a single-cell suspensions.

Cell labelling and sorting. All melanomas used in this study stably expressed DsRed and luciferase so that the melanoma cells could be unambiguously distinguished from mouse cells by flow cytometry and by bioluminescence imaging. When isolated by flow cytometry, cells were also stained with antibodies against mouse CD45 (30-F11-APC, eBiosciences), mouse CD31 (390-APC, Biolegend), Ter119 (TER-119-APC, eBiosciences) and human HLA-A, -B, -C (G46-2.6-FITC, BD Biosciences) to select live human melanoma cells and to exclude contaminating mouse endothelial and haematopoietic cells. Live human melanoma cells were thus isolated by flow cytometry by sorting cells that were positive for DsRed and HLA and negative for mouse CD45, Ter119 and CD31. All antibody labelling was performed for 20 min on ice, followed by washing and centrifugation. Before flow cytometric analysis, cells were re-suspended in staining medium (L15 medium containing bovine serum albumin (1 mg ml^{-1}), 1% penicillin/streptomycin, and 10 mM HEPES, pH 7.4) containing 4′,6-diamidino-2-phenylindole (DAPI; 5 μg ml^{-1}; Sigma) to eliminate dead cells from sorts and analyses. Sorts and analyses were performed using a FACSAria flow cytometer (Becton Dickinson). After sorting, an aliquot of sorted melanoma cells was always reanalysed to check for purity, which was usually greater than 95%. For analysis of circulating melanoma cells, blood was collected from each mouse by cardiac puncture with a syringe pretreated with citrate-dextrose solution (Sigma). Red blood cells were precipitated by Ficoll sedimentation according to the manufacturer's instructions (Ficoll Paque Plus, GE Healthcare). Remaining cells were washed with Hanks' balanced salt solution (Invitrogen) before antibody staining and flow cytometric analysis. For limiting dilution analysis, cells for each mouse were sorted into individual wells of 96-well V-bottomed plates containing staining medium and loaded into syringes directly from the well (one well into one syringe into one mouse).

Transplantation of melanoma cells. After sorting, cells were counted and resuspended in staining medium with 25% high-protein Matrigel (product 354248; BD Biosciences). Subcutaneous injections were performed into the right flank of NOD.CB17-*Prkdc*^{scid} *Il2rg*^{tm1Wjl}/SzJ (NSG) mice (Jackson Laboratory) in a final volume of 50 μl. Each mouse was transplanted with 100 melanoma cells unless otherwise specified. Tumour formation was evaluated regularly by palpation of the injection site, and the subcutaneous tumours were measured every 10 days until any tumour in the mouse cohort reached 2.5 cm in its largest diameter. Mice were monitored daily for signs of distress and euthanized when they exhibited distress according to a standard body condition score or within 24 h of their tumours reaching 2.5 cm in largest diameter, whichever came first. We adhered to this limit in all experiments. Organs were analysed visually and by bioluminescence imaging (see details below) for presence of macrometastases and micrometastases. These experiments were performed according to protocols approved by the Institutional Animal Care and Use Committee at the University of Texas Southwestern Medical Center (protocol 2011-0118). Intravenous injections were done by injecting cells into the tail vein of NSG mice in 100 μl of staining medium. For intrasplenic injections the mice were anaesthetized with isoflourane, then the left flank was shaved and disinfected with an ethanol wipe and iodine swab. An incision was made into the intraperitoneal cavity. The spleen was exposed with forceps and cells were injected slowly in a 40 μl volume of staining medium. The peritoneum was then sutured and skin was closed with clips. Mice were injected with buprenex before surgery and then again 12 h after surgery.

Lentiviral transduction of human melanoma cells. A bicistronic lentiviral construct carrying dsRed2 and luciferase (dsRed2-P2A-Luc) was generated (for bioluminescence imaging) and cloned into the FUW lentivrial expression construct. The primers that were used for generating this construct were: dsRed2 forward, 5′-CGACTCTAGAGGATCCatggatagcactgagaacgtc-3′ (capital letters indicate homology to FUW backbone); dsRed2 reverse, 5′-TCCACGTCTCCAGC CTGCTTCAGCAGGCTGAAGTTAGTAGCTCCGCTTCCctggaacaggtggtggc-3′ (capital letters indicate P2A sequences); luciferase forward, 5′-GCCTGCTG AAGCAGGCTGGAGACGTGGAGGAGAACCCTGGACCTGGATCCatggaag acgccaaaaacataaag-3′ (capital letters indicate P2A sequences) and luciferase reverse, 5′-GCTTGATATCGAATTCttacacggcgatctttccgc-3′ (capital letters indicate homology to FUW backbone). All constructs were generated using the In-Fusion HD cloning system (Clontech) and sequence verified.

For virus production, 0.9 μg of the appropriate plasmid and 1 μg of helper plasmids (0.4 μg pMD2G and 0.6 μg of psPAX2) were transfected into 293T cells using polyjet (Signagen) according to the manufacturer's instructions. Replication incompetent viral supernatants were collected 48 h after transfection and filtered through a 0.45- μm filter. Approximately 300,000 freshly dissociated melanoma cells were infected with viral supernatants supplemented with 10 μg ml^{-1} poybrene (Sigma) for 4 h. Cells were then washed twice with staining medium, and about 25,000 cells (a mixture of infected and non-infected cells) were suspended in staining medium with 25% high-protein Matrigel (product 354248; BD Biosciences) then injected subcutaneously into NSG mice. After growing to 1–2 cm in diameter, tumours were excised and dissociated into single-cell suspensions, and luciferase-dsRed^{+} or green fluorescent protein (GFP)$^{+}$ cells were collected by flow cytometry for injection into secondary recipients. Metastasis was monitored by bioluminescence imaging in secondary recipients. All shRNAs were expressed from a pGIPZ miRNA-based construct with TurboGFP from GE Dharmacon. For ALDH1L2, the following GE Dharmacon shRNA clones were used: V2LHS_30207, V2LHS_30209. For MTHFD1 the following GE Dharmacon shRNA clones were used: V2LHS_216208 and V2LHS_196832.

Bioluminescence imaging. Mice were injected with 100 luciferase-dsRed^{+} cells on the right flank and monitored until tumour diameters approached 2.5 cm, at which point they were imaged along with an uninjected control mouse using an IVIS Imaging System 200 Series (Caliper Life Sciences) with Living Image software. Mice were injected intraperitoneally with 100 μl of PBS containing D-luciferin monopotassium salt (40 μg ml^{-1}) (Biosynth) 5 min before imaging, followed by general anaesthesia 2 min before imaging. After imaging of the whole mouse, the mice were euthanized and individual organs were surgically removed and quickly imaged. The exposure time of images ranged from 10 to 60 s depending on signal intensity. The bioluminescence signal was quantified with 'region of interest' measurement tools in Living Image (Perkin Elmer) software. After imaging, tumours and organs were fixed in 10% neutral-buffered formalin for histopathology. For live imaging, mice were imaged once a month, and whole body bioluminescence was quantified using Living Image Software (Perkin Elmer).

LC–MS/MS metabolomic analysis. Mice were euthanized by cervical dislocation. Subcutaneous tumours and metastatic nodules were dissected, immediately homogenized in 80% methanol chilled with dry ice (Honeywell), vortexed vigorously, and metabolites were extracted overnight at −80 °C. The following day, samples were centrifuged at 13,000*g* for 15 min at 4 °C, the supernatant was collected, and metabolites from the pellet were re-extracted with 80% methanol at −80 °C for 4 h. After centrifugation, both supernatants were pooled and lyophilized using a SpeedVac (Thermo). To inhibit spontaneous oxidation, samples were extracted with 80% methanol containing 0.1% formic acid in some experiments[47]. Dried metabolites were reconstituted in 0.03% formic acid in water, vortexed and centrifuged, then the supernatant was analysed using liquid chromatography-tandem mass spectrometry (LC–MS/MS). A Nexera Ultra High Performance Liquid Chromatograph (UHPLC) system (Shimadzu) was used for liquid chromatography, with a Polar-RP HPLC column (150 × 2 mm, 4 μm, 80 Å, Phenomenex) and the following gradient: 0–3 min 100% mobile phase A; 3–15 min 100–0% A; 15–17 min 0% A; 17–18 min 0–100% A; 18–23 min 100% A. Mobile phase A was 0.03% formic acid in water. Mobile phase B was 0.03% formic acid in acetonitrile. The flow rate was 0.5 ml min^{-1} and the column temperature was 35 °C. A triple quadrupole mass spectrometer (AB Sciex QTRAP 5500) was used for metabolite detection as previously described[48]. Chromatogram peak areas were integrated using Multiquant (AB Sciex). To measure GSH and GSSG levels, some metabolite extractions were performed with 0.1% formic acid in 80% methanol, to inhibit spontaneous GSH oxidation. To calculate GSH and GSSG amounts, a standard curve was prepared by adding known quantities of GSH and GSSG to tumour metabolite extracts.

Isotope tracing with uniformly ^{13}C-labelled glucose. Mice were injected intraperitoneally with 2 g kg^{-1} body mass of uniformly ^{13}C-labelled glucose (Cambridge Isotopes) and were analysed 15, 30 and 60 min later. Mice were fasted for 14 h before the injection. In most experiments, subcutaneous tumours and metastatic nodules were surgically excised and homogenized in ice cold 50% methanol for GC–MS and in 80% dry ice-cold methanol for LC–MS analysis. Metabolites were extracted with three freeze-thaw cycles in liquid nitrogen. Supernatant was collected after a 15 min centrifugation at 13,000*g* at 4 °C and lyophilized. Metabolites were derivatized with trimethylsilyl (TMS) at 42 °C for 30 min for GC–MS analysis. ^{13}C-enrichment analysis was performed by GC–MS as previously described[48]. For LC–MS analysis, lyophilized samples were resuspended in either 0.03% formic acid in water or in 5 mM ammonium acetate in water depending on the method of analysis. For ^{13}C-enrichment analysis of

lactate, serine and glycine by LC–MS/MS, we used the liquid chromatography procedure described above for LC–MS/MS metabolomics analysis with the following modifications: the liquid chromatography gradient was 0–3 min 100% mobile phase A; 3–15 min 100–0% A; 15–17 min 0% A; 17–17.5 min 0–100% A; 17.5–20 min 100% A. For analysis of 3-PG, the liquid chromatography conditions were: mobile phase A, 5 mM ammonium acetate in water and mobile phase B, 5 mM ammonium acetate in acetonitrile, and a Fusion-RP HPLC column (150 × 2 mm, 4 μm, 80 Å, Phenomenex). The liquid chromatography gradient was: 0–3 min 100% mobile phase A; 3–9 min 100–0% A; 9–11 min 0% A; 11–12 min 0–100% A; 12–15 min 100% A. For metabolite detection a triple quadrupole mass spectrometer (AB Sciex QTRAP 5500) was used on multiple reaction monitoring mode as previously described, with some modifications[48]. The following transitions were used: positive mode: serine 106.1/60 (M + 1: 107.1/60 and 107.1/61, M + 2: 108.1/61 and 108.1/62, M + 3: 109.1/62), glycine 76/30 (M + 1 77/30 and 77/31, M + 2 78/31); negative mode: lactate 89/43 (M + 1 90/43 and 90/44, M + 2 91/44 and 91/45, M + 3 92/45), 3-PG 185/79 (M + 1 186/79, M + 2 187/79, M + 3 188/79) and 185/97 (M + 1 186/97, M + 2 187/97, M + 3 188/97). Unlabelled tissue was used as a negative control to confirm isotopic labelling in specific transitions.

Flow cytometric analysis of mitochondrial mass, mitochondrial membrane potential and ROS. Melanomas were generally dissociated enzymatically as described above. Equal numbers of dissociated cells (500,000–2,000,000) from subcutaneous tumours, Ficoll-depleted blood, or metastatic nodules were loaded with dyes to assess mitochondrial mass, mitochondrial membrane potential, and ROS levels. The dyes that were used to assess these parameters were all obtained from Life Technologies. We stained the dissociated cells for 20–45 min at 37 °C with 5 μM Mitotracker Green, Mitotracker DeepRed, CellROX Green, or CellROX DeepRed in HBSS-free (Ca^{2+}- and Mg^{2+}-free) to assess mitochondrial mass, mitochondrial membrane potential, mitochondrial and cytoplasmic ROS, respectively. For each indicator, staining intensity per cell was assessed by flow cytometry in live human melanoma cells (positive for human HLA and dsRed and negative for DAPI and mouse CD45/CD31/Ter119).

***In vivo* treatment of xenografts with drugs.** All animal experiments were performed according to protocols approved by the Institutional Animal Care and Use Committee at the University of Texas Southwestern Medical Center (protocol 2011-0118). Unless otherwise stated, 100 freshly dissociated melanoma cells were injected subcutaneously into the right flanks of NSG mice. When tumours became palpable, in some experiments mice were injected subcutaneously with NAC (Sigma, 200 mg kg^{-1} day^{-1} in 200 μl PBS, pH 7.4) or PBS as a control. Mice were injected with their last NAC dose 10 min before being euthanized for endpoint analysis. In experiments where mice received NAC via the drinking water, NAC was dissolved in PBS at 1 mg ml^{-1} and the water was changed every 2 days. In other experiments methotrexate (Tocris, 1.25 mg kg^{-1} day^{-1} in 100 μl PBS) was injected intraperitoneally 5 days per week. Mice that received methotrexate were simultaneously administered thymidine (Sigma, 3 mg per mouse per day in 100 μl PBS) and hypoxanthine (Sigma, 750 μg per mouse per day in 100 μl PBS) to prevent suppression of nucleotide biosynthesis. Tumour growth was monitored weekly with a caliper. Experiments were terminated when any tumour in the cohort reached 2.5 cm in size. At the end of experiments, blood was collected by cardiac puncture. Organs were analysed for micrometastases and macrometastases by bioluminescence imaging and visual inspection.

NADPH/$NADP^+$ measurement. Subcutaneous tumours or metastatic nodules were surgically excised as quickly as possible after euthanizing the mice then melanoma cells were mechanically dissociated and NADPH and $NADP^+$ were measured using NADPH/NADP Glo-Assay (Promega) following the manufactures instructions. Luminescence was measured using a using a FLUOstar Omega plate reader (BMG Labtech). Values were normalized to protein concentration, measured using a bicinchoninic acid (BCA) protein assay (Thermo).

Western blot analysis. Tissue lysates were prepared in Kontes tubes with disposable pestles using RIPA Buffer (Cell Signaling Technology) supplemented with phenylmethylsulfonyl fluoride (Sigma), and protease and phosphatase inhibitor cocktails (Roche). The BCA protein assay (Thermo) was used to quantify protein concentrations. Equal amounts of protein (15–30 μg) were separated on 4–20% Tris Glycine SDS gels (BioRad) and transferred to polyvinylidene difluoride membranes (BioRad). Membranes were blocked for 30 min at room temperature with 5% milk in TBS supplemented with 0.1% Tween20 (TBST) then incubated with primary antibodies overnight at 4 °C. After incubating with horseradish peroxidase conjugated secondary antibodies (Cell Signaling Technology), membranes were developed using SuperSignal West Pico or Femto chemiluminescence reagents (Thermo). Blots were stripped with 1% SDS, 25 mM glycine, pH 2, before re-probing. The following primary antibodies were used for western blot analyses: ALDH1L2 (LifeSpan Bio; LS-C178510), DHFR (LifeSpan Bio; LS-C138829), MTHFR (LifeSpan Bio; LS-C157974), SHMT1 (Cell Signaling; 12612S), SHMT2 (Cell Signaling; 12762S), MTHFD1 (ProteinTech; 10794-1-AP), MTHFD2 (ProtenTech; 12270-1-AP) and aActin (Abcam, ab8227).

Immunofluorescence staining of frozen tissue sections. Tissues were fixed in 4% paraformaldehyde for 12 h at 4 °C, and then transferred to 30% sucrose for 24 h for cryoprotection. Tissues were then frozen in OCT. Sections (10 μm) were permeabilized in PBS with 0.2% Triton (PBT), three times for 5 min each, and blocked in 5% goat serum in PBT for 30 min at room temperature. Sections were then stained with primary antibodies overnight: ALDH1L2 (LS-C178510, LifeSpan Bio; 1:50) and S100 (Z0311, Dako, 1:500). The next day, sections were washed in PBS with 0.2% Triton and stained with secondary goat anti-rabbit antibody (Invitrogen) at 1:500 for 30 min in the dark at room temperature. Sections were washed with PBT with DAPI (1:1,000) and mounted for imaging.

Statistical methods. No statistical methods were used to predetermine sample size. The data in most figure panels reflect several independent experiments performed on different days using melanomas derived from several patients. Variation is always indicated using standard deviation. For analysis of statistical significance, we first tested whether there was homogeneity of variation across treatments (as required for ANOVA) using Levene's test, or when only two conditions were compared, using the F-test. In cases where the variation significantly differed among treatments, the data were $\log_2$-transformed. If the data contained zero values, 1/2 of the smallest non-zero value was added to all measurements before log transformation. If the data contained negative values, all measurements were log-modulus transformed ($L(x) = \mathrm{sign}(x) \times \log(|x| + 1)$). In the rare cases when the transformed data continued to exhibit variation that significantly differed among treatments, we used a non-parametric Kruskal–Wallis test or a non-parametric Mann–Whitney test to assess the significance of differences among populations and treatments. Usually, variation did not significantly differ among treatments. Under those circumstances, two-tailed Student's *t*-tests were used to test the significance of differences between two treatments. When more than two treatments were compared, a one-way ANOVA followed by Dunnett's multiple comparisons tests were performed. A two-way ANOVA followed by Dunnett's multiple comparisons tests were used in cases where more than two groups were compared with repeated measures. Hierarchical clustering was performed using Euclidean distance in Metaboanalyst[49].

Mouse cages were randomized between treatments in all *in vivo* experiments (mice within the same cage had to be part of the same treatment). No blinding was used in any experiment. In all xenograft assays we injected 4–8-week-old NSG mice, 5 mice per treatment. Both male and female mice were used. For long-term assays, we injected 10 mice per treatment to account for non-melanoma related deaths (NSG mice are susceptible to death from opportunistic infections). When mice died before the end of experiments due to opportunistic infections the data from those mice were excluded. There were only two experiments in which this occurred. In Fig. 1c, d, 0–4 mice per melanoma line were found dead owing to an opportunistic bacterial infection before termination of the experiment and were excluded from the reported results. In Fig. 2b, 0–3 mice per melanoma line were found dead owing to opportunistic infections, before the first imaging time point after transplantation. These mice were excluded from the reported results.

47. Tu, B. P. *et al.* Cyclic changes in metabolic state during the life of a yeast cell. *Proc. Natl Acad. Sci. USA* **104,** 16886–16891 (2007).
48. Mullen, A. R. *et al.* Oxidation of α-ketoglutarate is required for reductive carboxylation in cancer cells with mitochondrial defects. *Cell Rep.* **7,** 1679–1690 (2014).
49. Xia, J., Mandal, R., Sinelnikov, I. V., Broadhurst, D. & Wishart, D. S. MetaboAnalyst 2.0–a comprehensive server for metabolomic data analysis. *Nucleic Acids Res.* **40,** W127–W133 (2012).

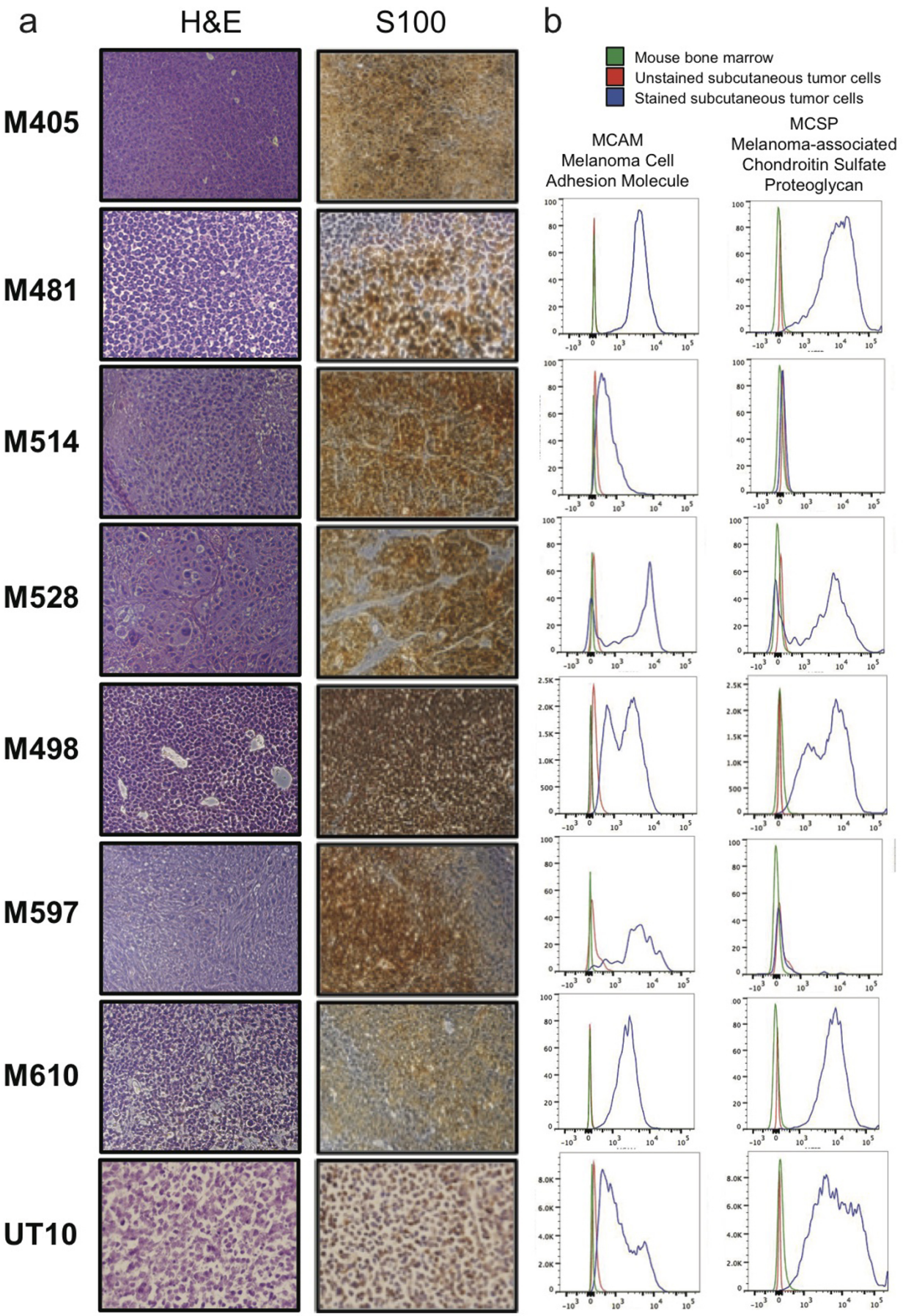

Extended Data Figure 1 | Expression of melanoma markers by xenografted melanomas. **a**, M405, M481, M514, M528, M498, M597, M610 and UT10 tumours were consistently positive for S100, a marker used clinically to diagnose melanoma. **b**, Flow cytometric analysis of xenografted tumour cells that were HLA-ABC^{+} and negative for mouse CD31/CD45/Ter119 showed that these cells were usually positive for melanoma cell adhesion molecule (MCAM) and melanoma-associated chondroitin sulphate proteoglycan (MCSP). Both of the tumours that lacked MCSP staining (M514 and M597) were heavily pigmented and expressed other melanoma markers (such as S100 and MCAM).

a

	melanoma ID	In Patient					In Mice	
		AT MELANOMA BANKING			AFTER MELANOMA BANKING		Micrometastases in organs other than lungs (% of xenografted mice)	Macrometastases (% of xenografted mice)
		AJCC Clinical Stage	Tumor site	Known Driver mutation	sites of distant metastasis	AJCC at death or at present		
Efficient	481	IIIB	Subcutaneous	BRAF V600E	Distant metastses to brain, lung, heart, mesentery, omentum, retroperitoneum, subcutaneous tissues and skeletal muscle	IV	78%	56%
Efficient	514	IIIC	Lymph Node	None	Distant metastases to multiple cutaneous/soft tissues and lung	IV	100%	42%
Efficient	405	IIIB	Lymph Node	NRAS Q61R	Distant metastses to cutaneous and mesenteric sites, lung, liver, spine, spleen, brain and pelvis	IV	96%	70%
Efficient	UT10	IIIC	Lymph Node	NRAS Q61K	Distant metastases to the brain, spine and lungs	IIIC	100%	95%
Inefficient	610	IIA	primary cutaneous	BRAF V600E	none	IIA	0%	0%
Inefficient	498	IIIB	primary cutaneous	None	none	unknown	0%	0%
Inefficient	528	IIIB	Lymph Node	BRAF V600E	none	IIIB	0%	0%
Inefficient	597	IIIA	primary cutaneous	None	none	IIIA	0%	0%

b

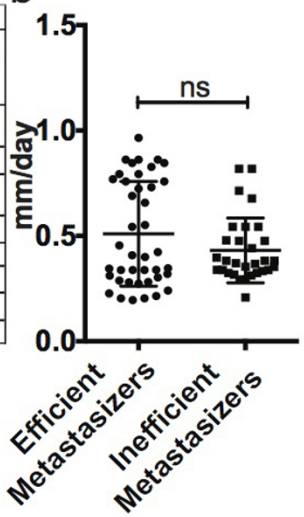

c

	melanoma ID	AT MELANOMA BANKING							AFTER MELANOMA BANKING			
		age/ sex	AJCC clinical stage	tumor site	prognostic information: primary thickness (mm)	prognostic information: primary tumor ulceration	prognostic information: Regional LN (#+)	prognostic information: visceral disease detected by scan? Y/N	therapy before banking	therapy after banking	sites of metastasis	survival (months after banking)	AJCC at death or at present
Efficient	481	67/M	IIIB	Subcutaneous	0.5mm (resected - 11y.)	Y	-	N	surgery	whole brain radiation, bortezomib	Brain, lung, heart, mesentery, omentum, retroperitoneum, subcutaneous tissues and left gluteus maximus muscle metastases	14.7	IV
Efficient	514	49/M	IIIC	Lymph Node	concurrent 16.0mm	Y	2	N	none	none	multiple cutaneous/soft tissue metastasis, lung	3.4	IV
Efficient	405	29/M	IIIB	Lymph Node	unknown	-	2	small brain nodule of uncertain etiology	none	IFN; IL-2	local/regional nodal recurrence, widespread soft tissue, cutaneous and mesenteric metastasis, lung, liver, spine, spleen, brain and pelvic metastases	12.4	IV
Efficient	UT10	65/M	IIIC	Upper extremity axillary nodal metastasis	unknown	-	1	Y	none	IL-2, Ipilimumab	Distant metastases to the brain, spine and lungs	22	IIIC
Inefficient	498	83/M	IIIB	primary cutaneous	5.3mm	N	-	N	none	radiation	none	70 death from unknown cause)	unknown
Inefficient	528	72/M	IIIB		unknown	-	1	lung masses (not melanoma)	none	chemotherapy	none	40.7 death from lung cancer)	IIIB
Inefficient	610	76/F	IIA	primary cutaneous	3.5mm	N	-	-	none	unknown	none	8.9 (death unrelated to melanoma)	unknown
Inefficient	597	61/M	IIIA	primary cutaneous	Clark Level V	N	0	N	none	none	none	>36	IIIA

Extended Data Figure 2 | Clinical data on the melanomas used in this study and summary of their metastatic behaviour in NSG mice. **a**, Summary of the clinical characteristics of the melanomas used in this study at the time of banking, as well as patient outcome after banking, and metastasis patterns upon transplantation of banked tumours into NSG mice. Melanomas were stratified into efficiently and inefficiently metastasizing melanomas. Efficiently metastasizing melanomas formed distant metastases in patients and in NSG mice, whereas inefficiently metastasizing melanomas did not. The latter group did form micrometastases in the lung, but not outside of the lung in the period of time it took for subcutaneous tumours to grow to 2 cm in diameter (when the mice had to be euthanized in these experiments[27]). Nonetheless, most of the inefficiently metastasizing melanomas have the ability to form macrometastases if given enough time (data not shown). **b**, Growth rates of subcutaneous tumours in NSG mice after subcutaneous transplantation of 100 cells. Statistical significance was assessed using two-tailed Student's *t*-test. **c**, Clinical characteristics of the patients from whom melanomas were obtained at the time of banking and upon subsequent clinical follow up. The tumours were confirmed to be melanomas by clinical dermatopathology. The tumours were independently confirmed to be melanomas after xenografting in mice by histological and flow cytometric analysis of melanoma markers (Extended Data Fig. 1) as well as examination by a clinical dermatopathologist.

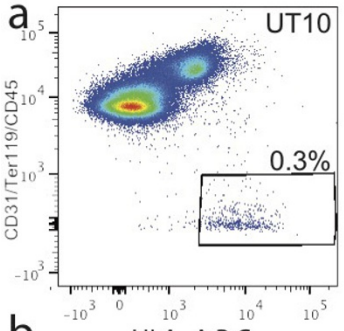

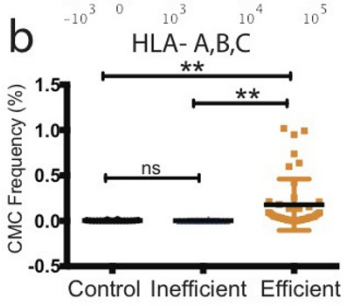

Legend for figure 1 (c-f)

Total flux (photon/sec)

- < 10^6
- 10^6 - 10^7
- 10^7 - 10^8
- >10^8
- x Macrometastases

c Efficient Metastasizers

Melanoma	Cell Dose	Lung	Liver	Kidney	Pancreas /Spleen	Gut
M481	10000	x	x			
	10000					
	10000	x	x			
	10000					
	1000					
	1000					
	1000	x	x			
	1000					
	1000	x	x	x	x	
	100	x	x			
	100					
	100	x	x		x	
	100	x	x	x	x	x
	100	x	x	x	x	
	100		x	x	x	x
	10					
	10					
	10					
M405	1000	x	x	x	x	x
	1000	x	x	x	x	x
	100					
	100					
	100					
	100	x	x	x		x
	10					
	10					
	10					
M514	1000					
	1000	x	x	x	x	x
	100	x	x	x	x	x
	100	x				
	10					
	10					
	10					
UT10	1000	x	x	x	x	x
	1000	x	x	x	x	x
	1000	x	x	x	x	x
	1000					
	1000	x	x	x	x	x
	100					
	100					
	100					
	100					
	100					

d Inefficient Metastasizers

Melanoma	Cell Dose	Lung	Liver	Kidney	Pancreas/ Spleen	Gut
M528	10000					
	10000					
	1000					
	1000					
	1000					
	100					
	100					
	100					
	100					
	100					
	100	x				
	10					
	10					
	10					
	10					
M610	1000					
	100					
	100					
	100					
	10					
	10					
	10					
M498/ M499	1000					
	1000					
	100					
	100					
	100					
	100					
	100					
	10					
M597	1000					
	1000					
	100					
	100					
	100					

e Efficient Metastasizers

Melanoma	Cell Dose	Lung	Liver	Kidney	Pancreas/Spleen	Gut
M481	1000		x	x	x	x
	1000		x	x	x	x
	100					
	100		x	x	x	x
	10					
	10	x	x	x	x	x
M405	1000		x			
	100					
	100					
	100					
	100					
	10					
	10					
	10					
M514	1000		x	x	x	x
	100		x		x	x
	100		x			
	10					
	10					

f Inefficient Metastasizers

Melanoma	Cell Dose	Lung	Liver	Kidney	Pancreas/Spleen	Gut
M610	1000					
	1000		x			
	1000					
	1000					
	100					
	100					
	100					
	10					
	10					
M528	100					
	100					
	10					
	10					
	10					
M498	1000					
	1000					
	1000					
	100					
	100					
	100					
	10					
	10		x	x	x	x
	10					

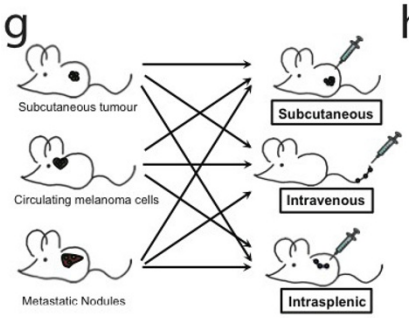

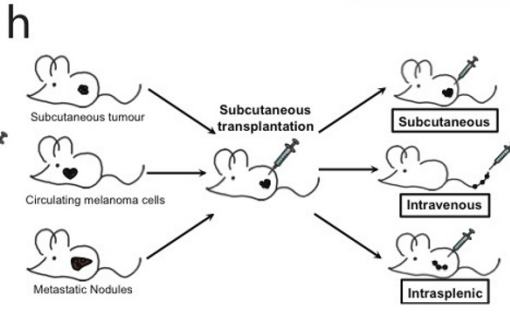

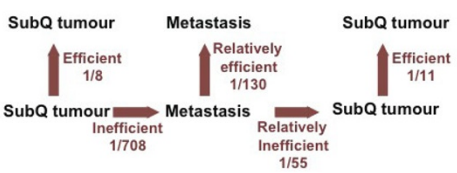

Extended Data Figure 3 | Barriers to distant metastasis *in vivo*. **a**, Live human melanoma cells were identified by flow cytometry based on the expression of DsRed (all melanomas in this study stably expressed DsRed) and human HLA and the lack of expression of mouse CD45, CD31 and Ter119 (to exclude mouse haematopoietic and endothelial cells). Human melanoma cells were observed in the blood of NSG mice bearing efficiently metastasizing melanomas. **b**, Mice xenografted with efficiently metastasizing melanomas ($n = 43$ mice with tumours derived from four patients) had significantly higher frequencies of CMCs in their blood than mice xenografted with inefficiently metastasizing melanomas ($n = 13$ mice with tumours derived from four patients) or control mice that had not been xenografted ($n = 18$ mice). Blood was collected by cardiac puncture. Statistical significance was assessed using ANOVA followed by Tukey's test for multiple comparisons. $^{**}P < 0.005$. **c**–**f**, Bioluminescence analysis of total photon flux (photons s^{-1}) from mouse organs after intravenous injection (**c**, **d**) or intrasplenic injection (**e**, **f**) of luciferase-tagged melanoma cells derived from efficiently metastasizing (**c**, **e**) or inefficiently metastasizing (**d**, **f**) melanomas. Each melanoma was derived from a different patient and was studied in an independent experiment. **g**, Schematic of the experiment shown in Table 2a. **h**, Schematic of the experiment shown in Table 2b. **i**, Summary of mean limiting dilution frequencies of tumour-forming cells after subcutaneous, intravenous, or intrasplenic transplantation into NSG mice.

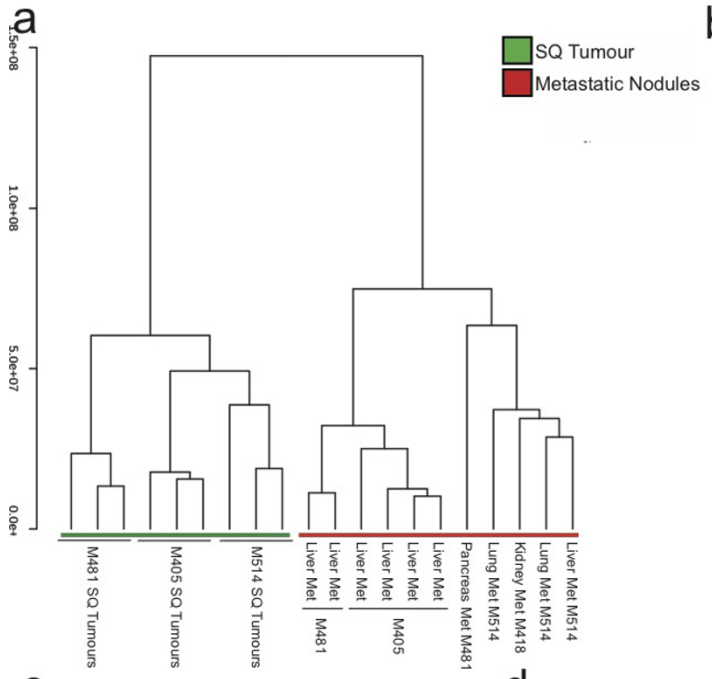

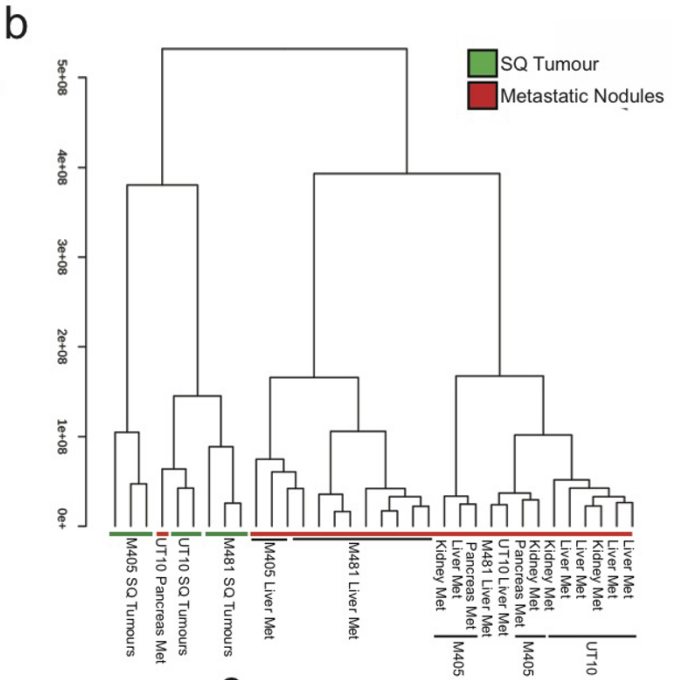

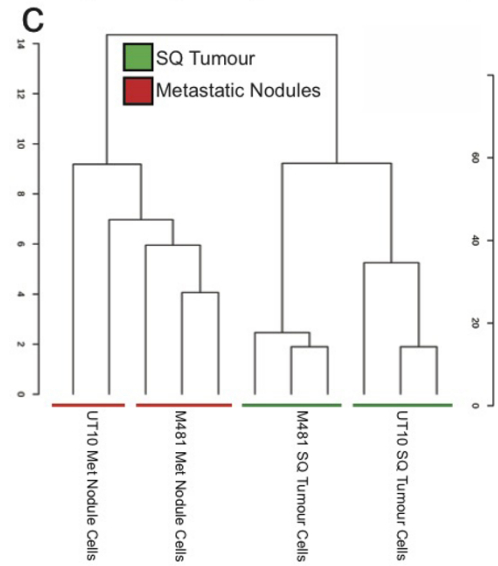

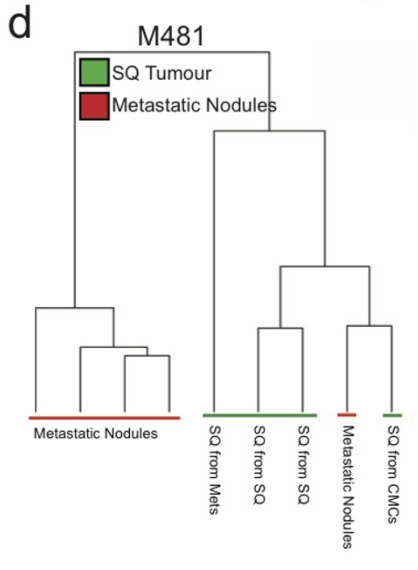

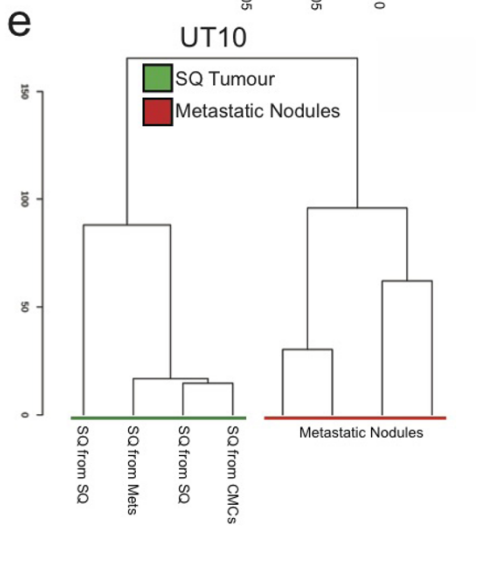

f

	Experiment	Figure Panel	GSH/GSSG in SQ Tumour	GSH/GSSG in metastasizing cells	p-value
i	Tumour GSH/GSSG measurement with FA	Figure 1a	270	140	0.0046
ii	Tumour Metabolomics #1	Extended Figure 4a	170	20	0.0006
iii	Tumour Metabolomics #2	Extended Figure 4b	26	8.1	0.0031
iv	Circulating melanoma cell metabolomics	Figure 1b	19	4.5	0.0027
v	Sorted Cell Metabolomics with FA	Extended Figure 4c	44	38	0.0186

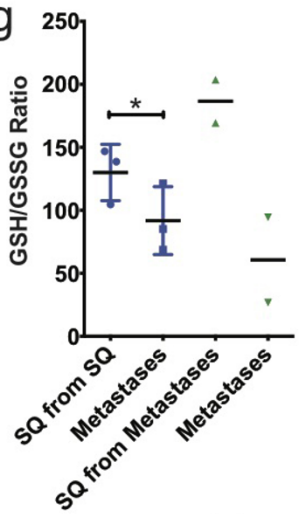

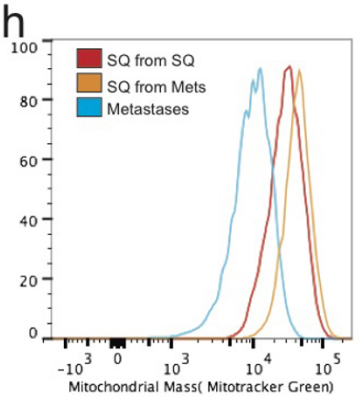

Extended Data Figure 4 | Unsupervised clustering suggests that melanoma cells undergo reversible metabolic changes during metastasis. **a**, **b**, Hierarchical clustering from two independent experiments reflecting subcutaneous tumours and metastatic nodules from the liver, pancreas, lung and kidneys of mice transplanted with melanomas M405, M481 and M514 (**a**) (see Extended Data Table 1 for data on individual metabolites) and subcutaneous tumours and metastatic nodules from the liver, pancreas and kidneys of mice transplanted with melanomas M405, M481 and UT10 ($n = 2$–3 mice per melanoma in each experiment; see Extended Data Table 2 for data on individual metabolites) (**b**). **c**, Hierarchical clustering of metabolites extracted from flow cytometrically sorted human melanoma cells isolated from subcutaneous tumours or metastatic nodules (UT10, M481, $n = 3$ mice per melanoma in two independent experiments). **d**, **e**, Hierarchical clustering of metabolites extracted from subcutaneous tumours and metastatic nodules from mice transplanted subcutaneously with either subcutaneous, circulating or metastatic melanoma cells ($n = 4$ mice for each melanoma in two independent experiments). **f**, GSH/GSSG ratios from each of the experiments that compared subcutaneous tumours and metastasizing cells. (i) Metabolites were extracted in the presence of 0.1% formic acid to inhibit spontaneous oxidation[42] in two independent experiments comparing subcutaneous and metastatic tumours from mice with three different melanomas in each experiment (M405, M481 and UT10). (ii) and (iii) GSH/GSSG ratios from the experiments shown in **a** and **b**, respectively. (iv) GSH/GSSG ratios in melanoma cells isolated by flow cytometry from subcutaneous tumours and the blood (circulating melanoma cells) of mice bearing M405 and M481. (v) Metabolites were extracted in the presence of 0.1% formic acid in two independent experiments in which melanoma cells were isolated by flow cytometry from subcutaneous and metastatic tumours (M405 and M481). While the GSH/GSSG ratio was always significantly higher in melanoma cells from subcutaneous tumours as compared to circulating cells or metastatic nodules the ratio varied among experiments as a result of technical differences in cell isolation and metabolite extraction as well as differences in mass spectrometry sensitivity to GSH and GSSG. **g**, GSH/GSSG ratios in subcutaneous tumours that arose from the transplantation of melanoma cells obtained from subcutaneous tumours or metastatic nodules, as well as the metastatic nodules from the same mice (M405; $n = 2$ to 3 mice per treatment in one experiment). These data suggest that the decline in GSH/GSSG ratio in metastasizing melanoma cells is reversible upon subcutaneous transplantation. **h**, Histogram showing mitochondrial mass in subcutaneous tumour cells that arose from the transplantation of subcutaneous cells (SQ from SQ), subcutaneous tumour cells that arose from the transplantation of metastatic cells (SQ from Mets), and metastatic cells (metastases). These histograms reflect the data shown in Fig. 1g. All error bars represent s.d. Statistical significance was assessed using, two-tailed Student's *t*-tests (**f** and **g**). $*P < 0.05$.

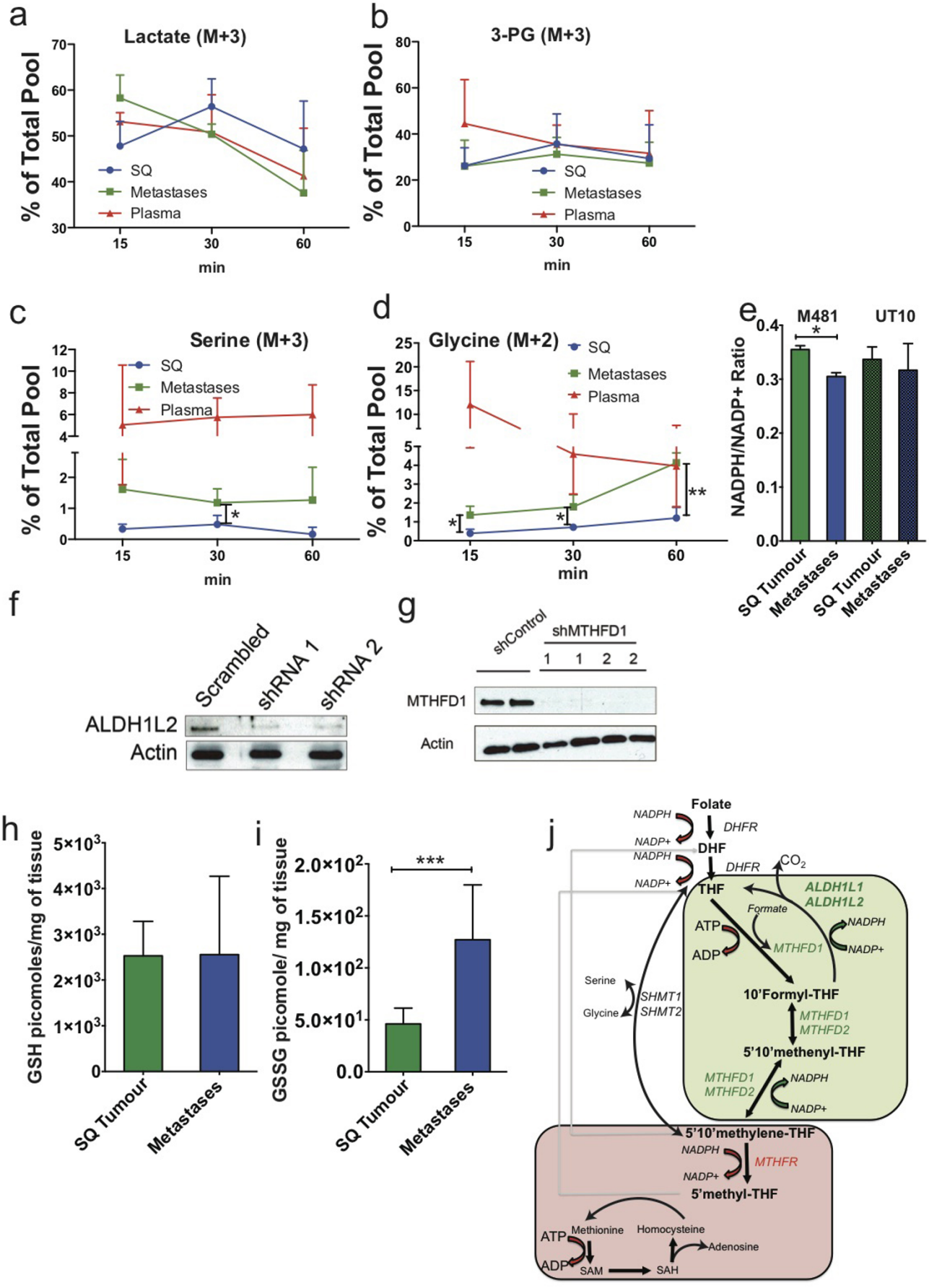

Extended Data Figure 5 | Metastatic nodules exhibited increased enrichment of labelled serine and glycine as compared to subcutaneous tumours. *In vivo* isotope tracing of uniformly ^{13}C-labelled lactate (M + 3) (**a**), 3-phosphoglycerate (M + 3) (**b**), serine (M + 3) (**c**), and glycine (M + 2) (**d**) in subcutaneous tumours versus metastatic nodules from the same mice (UT10, $n = 3$–4 mice per time point in two independent experiments). The fractional enrichment of labelled lactate, and 3-PG did not significantly differ among plasma, subcutaneous tumours or metastatic tumours at any time point. By contrast, the fractional enrichment of labelled serine and glycine were significantly higher in metastatic as compared to subcutaneous tumours. This is consistent with increased *de novo* serine synthesis in metastatic tumours but could also reflect altered serine/glycine exchange with circulating serine/glycine pools in metastatic as compared to subcutaneous tumours. **e**, NADPH/NADP ratios in subcutaneous tumours and metastatic nodules from the same mice shown in Fig. 2d, e. **f**, **g**, Western blot of ALDH1L2 (**f**) and MTHFD1 (**g**) protein after shRNA knockdown in melanoma cells. Uncropped western blots are shown in Supplementary Fig. 1. **h**, **i**, Amount of GSH (**h**) and GSSG (**i**) per mg of subcutaneous or metastatic tumour as measured by LC–MS (M405, M481 and UT10, $n = 2$–3 mice per melanoma in two independent experiments). All data represent mean ± s.d. Statistical significance was assessed using two-tailed Student's *t*-tests (**e**, **h** and **i**) and one-way ANOVAs followed by Dunnett's tests for multiple comparisons (**a**–**d**). $*P < 0.05$; $***P < 0.0005$. **j**, Schematic of the folate pathway including NADPH generating (green box) and NADPH consuming (red box) reactions.

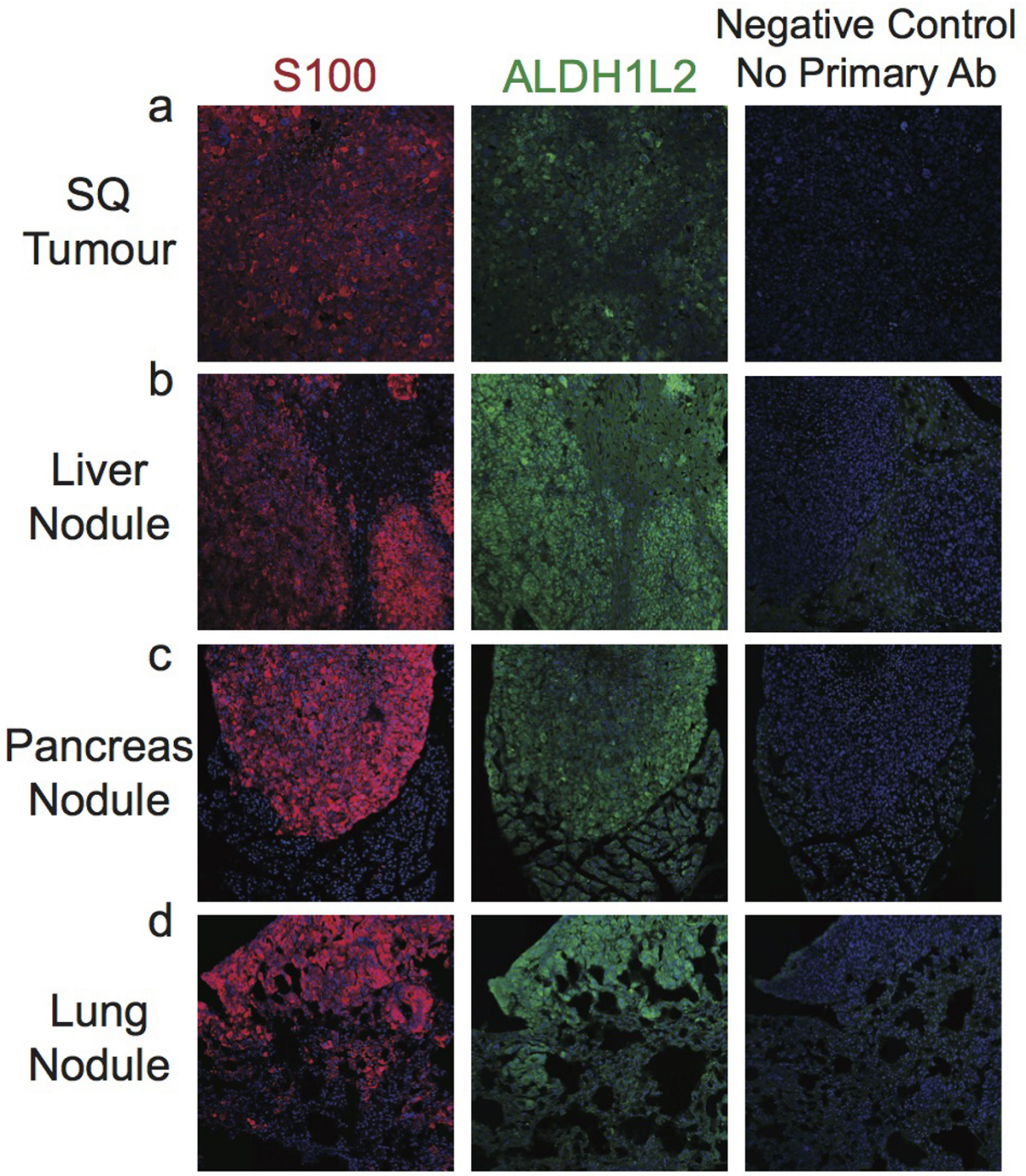

Extended Data Figure 6 | Immunofluorescence analysis of ALDH1L2 in subcutaneous melanoma as well as metastatic nodules in the liver, pancreas and lung. a–d, Melanoma cells can be distinguished from host stromal cells based on staining for the melanoma marker, S100.

Extended Data Table 1 | Fold change and statistical significance corrected for multiple comparisons of metabolites detected by LC–MS/MS in the experiment in Extended Data Fig. 2a.

Metabolite	Fold Change of Metastasis/SQ Tumor	FDR	Metabolite	Fold Change of Metastasis/SQ Tumor	FDR
citraconic acid/ketohexanoic acid	12.311	0.054768	tyrosine	0.82787	0.47274
glucarate	11.472	0.13347	leucine	0.82491	0.29642
sedoheptulose 7-phosphate	5.6121	0.084567	citrulline	0.82483	0.44062
GABA	4.8296	0.44062	S-lactoylglutathione	0.81622	0.78839
betaine	4.8132	6.12E-05	guanosine	0.81517	0.55117
AICAR	4.5004	0.15975	pyroglutamic acid	0.81294	0.61138
carnitine-C18	4.4942	0.13347	GMP	0.81159	0.64286
spermidine	4.4416	0.016469	3-hydroxybutyrate	0.80538	0.72186
adenosine 5-diphosphoribose	4.1336	0.041494	hydroxyphenylpyruvate	0.798	0.26547
xanthosine	3.9645	0.11311	glycerate	0.77694	0.66141
glutamine	3.9371	0.000419	phenyllactic acid	0.77196	0.02971
hexose-phosphate	3.0656	0.086761	homoserine/threonine	0.7596	0.44062
GSSG	2.8724	0.081173	methionine	0.74125	0.28847
S-methyl-5-thioadenosine	2.8234	0.21534	carnitine	0.73503	0.38386
gluconate	2.7963	0.052588	cADP-ribose	0.73299	0.12096
xanthine	2.4873	0.084567	O-acetylserine	0.72801	0.19553
pyridoxamine	2.4531	0.24821	homocysteine	0.72727	0.16015
spermine	2.3796	0.19553	methylglyoxal	0.72483	0.08875
aminoadipic acid	2.3513	0.44062	creatine	0.72291	0.24821
carnitine-C16	2.3105	0.27824	fumarate	0.7092	0.17141
uridine	2.2733	0.13025	lactate	0.70716	0.13819
citrate	2.1797	0.081173	proline	0.69532	0.27038
methionine sulfoxide	2.0674	0.22847	alpha-ketoisovaleric acid	0.6943	0.14034
ribose 5-phosphate	2.0193	0.40173	cystathionine	0.6937	0.56124
glycerol 3-phosphate	2.0132	0.40173	UMP	0.67863	0.13819
IMP	1.987	0.018053	carbamoylphosphate	0.67623	0.33231
S-adenosylmethionine	1.8423	0.17083	N-acetylglucosamine phosphate	0.65886	0.05477
inosine	1.8253	0.24736	carnitine-C4	0.63354	0.52908
riboflavin	1.7888	0.19553	CMP	0.60248	0.11112
hypoxanthine	1.6282	0.23352	orotate	0.60141	0.15634
acetyllysine	1.5539	0.5435	pipecolic acid	0.6	0.05259
NAD	1.5512	0.47123	fructose	0.59758	0.09166
taurine	1.5405	0.21332	adenine	0.59213	0.03863
thiamine	1.4869	0.47274	hydroxyproline	0.59052	0.00051
aspartate	1.3202	0.68641	GSH	0.58564	0.12364
putrescine	1.3107	0.64286	pantothenic acid	0.57614	0.11592
kynurenine	1.2857	0.56968	cytidine	0.54462	0.05231
dAMP	1.2535	0.61138	phospho-hydroxybenzoate	0.53605	0.31067
thymidine	1.2419	0.6972	phosphocholine	0.53561	0.06755
ornithine	1.2218	0.70841	propionylcholine	0.53061	0.13303
phenylalanine	1.2154	0.49828	1-methyladenosine	0.52411	0.00529
AMP	1.2057	0.69525	glutamate	0.48917	0.01647
S-adenosylhomocysteine	1.1992	0.77036	N-acetylaspartate	0.48911	0.15634
acetylcarnitine	1.1403	0.68641	hydroxyglutarate	0.48629	0.01468
trimethyllysine	1.1395	0.83403	acetylcholine	0.48281	0.03065
carnitine-C8	1.1074	0.78839	shikimic acid	0.46778	0.05604
carnitine-C3	1.0818	0.83403	phosphocreatine	0.46674	0.13819
asparagine	1.0678	0.72161	carnitine-C5	0.45886	0.19875
choline	1.0661	0.83403	alpha-ketoglutarate	0.4554	0.08972
malate	1.0497	0.78839	arginine	0.44217	0.02915
glycerophosphorylcholine	1.0439	0.9381	2-deoxycytidine	0.43995	0.23352
1-methylhistidine	1.0248	0.9381	uracil	0.43712	0.01468
nicotinamide	1.0018	0.99511	5-aminolevulinic acid	0.436	0.00012
glyoxylate	0.98478	0.9381	nicotinate	0.4316	0.19553
dimethylglycine	0.97783	0.91723	lysine	0.40191	6.12E-05
glycine	0.94707	0.91453	1-methylnicotinamide	0.39599	0.33556
succinate	0.94473	0.83403	N,N-dimethylarginine	0.38777	0.00093
alanine	0.92949	0.78839	carnitine-C14	0.3696	0.24821
carnitine-C6	0.92856	0.83403	myo-inositol	0.34547	0.13347
indole	0.92843	0.83403	creatinine	0.29845	0.00047
tryptophan	0.92275	0.80122	ascorbic acid	0.25524	1.57E-06
urea	0.90704	0.66141	XMP	0.15598	0.06755
Guanidoacetic acid	0.88659	0.70463	carnitine-C12	0.15514	0.09166
histidine	0.86073	0.67732	ADP	0.071143	2.54E-07
valine	0.8468	0.66141			

Extended Data Table 2 | Fold change and statistical significance corrected for multiple comparisons of metabolites detected by LC–MS/MS in the experiment shown in Extended Data Fig. 2b.

Metabolite	Fold Change Metastasis/SQ Tumor	FDR	Metabolite	Fold Change Metastasis/SQ Tumor	FDR
citraconic acid/ketohexanoic acid	34.483	0.45284	methionine sulfoxide	0.90754	0.71378
carnitine-C18	10.963	0.02495	citrulline	0.90545	0.69494
NADP	10.741	0.02463	leucine	0.90323	0.39527
adenosine 5-diphosphoribose	6.9242	0.01199	GSH	0.88817	0.69787
carnitine-C16	4.962	0.03569	S-methyl-5-thioadenosine	0.87643	0.60788
hypoxanthine	4.8303	0.01049	putrescine	0.87293	0.3561
pyridoxamine	4.7958	0.02923	cysteine	0.86437	0.7895
betaine	4.7812	0.03627	3-hydroxybutyrate	0.86329	0.5511
S-adenosylhomocysteine	4.3483	0.01917	N-acetylaspartate	0.78325	0.48791
gluconate	4.2564	0.03675	serine	0.78075	0.79908
xanthine	4.1876	0.00192	alanine	0.76685	0.11668
GSSG	4.0565	0.00339	carnitine-C14	0.76026	0.70454
AICAR	3.8575	0.02826	GMP	0.74002	0.18657
xanthosine	3.7994	0.07897	histidine	0.72959	0.0396
adenosine	3.555	0.00983	O-acetylserine	0.72727	0.01269
uridine	3.497	9.33E-05	glutamate	0.72558	0.14273
glutamine	3.318	0.01391	acetylcarnitine	0.68306	0.00192
aconitate	3.2415	0.04627	2-deoxycytidine	0.67868	0.29585
sedoheptulose 7-phosphate	2.9576	0.19981	ascorbic acid	0.67473	0.28456
NAD	2.9139	0.00151	carnitine-C12	0.67254	0.5056
riboflavin	2.8081	0.0222	lactate	0.65954	0.00047
adenosine	2.7184	0.00181	choline	0.65842	0.00389
guanosine	2.4328	0.01321	acetylcholine	0.6573	0.13515
ZMP	2.4059	0.12097	creatinine	0.6543	0.16525
inosine	2.3785	0.14043	y-aminobutyric acid	0.64139	0.2191
IMP	2.3314	0.01049	glucose/fructose	0.63849	0.00925
deoxyinosine	2.2956	0.20059	homoserine/threonine	0.62876	0.02462
uridine	2.2759	0.01549	dimethylglycine	0.62167	0.00068
SAICA	2.0448	0.13492	carnitine-C4	0.59432	0.16312
malate	1.9365	1.81E-06	N-acetylglucosamine phosphate	0.59273	0.00095
aminoadipic acid	1.9042	0.01321	glucuronate	0.57813	0.00338
carnitine-C8	1.8744	0.0222	UMP	0.57702	0.0163
kynurenine	1.869	0.00672	uridine 5-diphosphoglucuronic acid	0.57518	0.02632
dAMP	1.802	0.00099	phenyllactic acid	0.57402	0.00024
fructose 6-phosphate	1.7965	0.26537	N,N-dimethylarginine	0.5534	0.00047
thymidine	1.6716	0.27532	propionylcholine	0.55055	0.00853
cADP-ribose	1.5868	0.0663	allantoin	0.54186	2.44E-05
cytidine	1.5195	0.21432	urea	0.52852	7.29E-07
carnitine-C6	1.512	0.08539	1-methylnicotinamide	0.51941	0.02008
S-lactoylglutathione	1.46	0.6708	5-aminolevulinic acid	0.51688	8.12E-05
glycerol 3-phosphate	1.4129	0.42166	deoxyribose phosphate	0.50607	0.01321
7-methylguanosine	1.4076	0.55385	uracil	0.50113	0.06104
glyoxylate	1.3983	0.00203	carnitine	0.49567	1.66E-07
S-adenosylmethionine	1.3577	0.15136	taurine	0.46303	2.17E-05
glycerophosphorylcholine	1.335	0.16611	cytosine	0.45951	6.21E-07
tryptophan	1.318	0.19633	proline	0.4591	4.23E-06
1-methyladenosine	1.2813	0.03412	carnitine-C5	0.44249	0.00483
AMP	1.2804	0.43896	ornithine	0.43836	0.00505
citrate	1.2214	0.67146	1-methylhistidine	0.4023	2.31E-06
nicotinamide	1.2063	0.62079	uracil	0.3904	0.01116
succinate	1.196	0.50829	creatine	0.37961	1.26E-07
hydroxyphenylpyruvate	1.1937	0.26901	trimethyllysine	0.37893	7.58E-05
phenylalanine	1.1838	0.1462	arginine	0.36929	0.00047
carnitine-C3	1.1524	0.54363	CMP	0.36814	3.24E-09
tyrosine	1.1166	0.50877	phosphocholine	0.36461	7.43E-09
methionine	1.0869	0.70454	alpha-ketoglutarate	0.35719	0.02197
2-aminooctanoic acid	1.0803	0.71185	spermidine	0.35496	0.03329
adenine	1.0676	0.74371	acetyllysine	0.35375	3.01E-05
asparagine	1.0509	0.69494	phosphocreatine	0.34497	0.00048
pipecolic acid	1.0216	0.96295	agmatine	0.32422	8.26E-06
thiamine	1.0179	0.97565	hydroxyglutarate	0.30783	3.24E-09
ribose 5-phosphate	1.0132	0.97843	lysine	0.27436	3.91E-10
homocysteic acid	1.0076	0.97843	phosphoenolpyruvic acid	0.27364	1.99E-08
fumarate	1.0022	0.9897	XMP	0.2693	4.33E-05
indole	1.0017	0.9897	cystathionine	0.26823	0.02462
pantothenic acid	0.97947	0.9674	glycine	0.24469	3.32E-09
homocysteine	0.97252	0.96295	carbamoylphosphate	0.17283	8.74E-09
Guanidoacetic acid	0.97007	0.79908	myo-inositol	0.14292	5.08E-07
valine	0.94431	0.69728	cadaverine	0.06894	0.09355
orotate	0.93458	0.90099	nicotinate	0.066878	0.12347

Extended Data Table 3 | Treatment with the antioxidant NAC increased tumour formation by intravenously transplanted melanoma cells.

a

Efficient Metastasizers					
		Cell Dose	Mice Injected	Mice that formed tumours	Frequency of tumour-forming cells
Total	With NAC	1000	15	13	1/443 ****
		100	15	4	
	Without NAC	1000	15	3	1/4983 ****
		100	15	0	

b

Inefficient Metastasizers					
		Cell Dose	Mice Injected	Mice that formed tumours	Frequency of tumour-forming cells
Total	With NAC	10000	5	2	1/16157
		1000	10	1	
		100	10	0	
	Without NAC	10000	5	0	-
		1000	10	0	
		100	10	0	

Limiting dilution analysis of tumour formation by intravenously transplanted efficiently metastasizing (**a**, M405, M481 and UT10) or inefficiently metastasizing (**b**, M528 and M597) melanoma cells. In half the mice, the cells were pre-treated with NAC before transplantation and the mice were maintained on water supplemented with NAC after transplantation ($n = 5$ mice/treatment/melanoma for a total of 110 mice in five independent experiments). Statistical significance was assessed by a Chi-square test using ELDA software[46]. ****$P < 0.00005$.

Extended Data Table 4 | Fold increase in metastatic nodules as compared to subcutaneous tumours of transcripts involved in antioxidant responses and NADPH generation.

Gene Name	Gene	Metastatic/Subcutaneous (Fold Change)	p-value*
GCLC	Glutamate-cysteine ligase (catalytic subunit)	1.20	0.560
GCLM	Glutamate-cysteine ligase (modifier subunit)	0.86	0.300
GSS	Glutathione synthase	0.90	0.240
SOD1	Superoxide disumutase 1	1.09	0.355
SOD2	Superoxide dismutase 2	0.86	0.454
SOD3	Superoxide dismutase 3	0.64	0.189
CAT	Catalase	1.09	0.548
GPX1	Glutathione Peroxidase 1	1.30	0.117
GPX2	Glutathione Peroxidase 2	1.00	0.998
GPX3	Glutathione Peroxidase 3	0.40	0.048
GPX4	Glutathione Peroxidase 4	1.07	0.459
GPX7	Glutathione Peroxidase 7	0.83	0.183
GPX8	Glutathione Peroxidase 8	0.87	0.631
GSR	Glutathione Reductase	1.12	0.372
HMOX1	Heme Oxygenase 1	0.86	0.186
HMOX2	Heme Oxygenase 2	1.41	0.008
TXN	Thioredoxin 1	1.16	0.297
TXN2	Thioredoxin 2	1.15	0.480
TXNRD1	Thioredoxin reductase 1	0.97	0.859
TXNRD2	Thioredoxin reductase 2	0.91	0.701
TXNRD3	Thioredoxin reductase 3	1.15	0.176
PRDX1	Peroxiredoxin 1	1.67	0.334
PRDX2	Peroxiredoxin 2	0.94	0.289
PRDX3	Peroxiredoxin 3	1.31	0.013
PRDX4	Peroxiredoxin 4	1.13	0.075
PRDX5	Peroxiredoxin 5	1.28	0.032
PRDX6	Peroxiredoxin 6	1.05	0.172
NFE2L2	Nuclear factor, erythroid 2-like 2	0.90	0.106
G6PD	Glucose-6-phosphate Dehydrogenase	2.20	0.156
PGD	Phosphogluconate dehydrogenase	0.98	0.758
ME2	Malic Enzyme 2	1.05	0.865
CBS	Cystathione beta Synthase	1.20	0.469

Data are based on RNA sequencing (RNA-seq) analysis of two subcutaneous tumours and two metastatic nodules for each of M405 and M481.